⑫

UNCLASSIFIED

AD-A185 785

. REPORT DOCUMENTATION PAGE		Form Approved OMB No. 0704-0188

1a REPORT SECURITY CLASSIFICATION UNCLASSIFIED	1b RESTRICTIVE MARKINGS

2a SECURITY CLASSIFICATION AUTHORITY	3 DISTRIBUTION/AVAILABILITY OF REPORT Approved for public release; distribution unlimited.
2b DECLASSIFICATION/DOWNGRADING SCHEDULE	

DTIC SELECTED NOV 1 0 1987 S D

4 PERFORMING ORGANIZATION REPORT NUMBER(S) N00014-85-C-0141-AR7	5. MONITORING ORGANIZATION REPORT NUMBER(S) .

6a NAME OF PERFORMING ORGANIZATION Washington State University	6b OFFICE SYMBOL (If applicable)	7a. NAME OF MONITORING ORGANIZATION Office of Naval Research

6c. ADDRESS (City, State, and ZIP Code) Department of Physics Washington State University Pullman, WA 99164-2814	7b. ADDRESS (City, State, and ZIP Code) Physics Division--Code 1112 Arlington, VA 22217-5000

8a. NAME OF FUNDING/SPONSORING ORGANIZATION	8b. OFFICE SYMBOL (If applicable)	9 PROCUREMENT INSTRUMENT IDENTIFICATION NUMBER N00014-85-C-0141

| 8c. ADDRESS (City, State, and ZIP Code) | 10 SOURCE OF FUNDING NUMBERS |

PROGRAM ELEMENT NO.	PROJECT NO.	TASK NO.	WORK UNIT ACCESSION NO.
61153N11		4126934	

11 TITLE (Include Security Classification)
Research on Acoustical Scattering, Diffraction Catastrophes, Optics of Bubbles, Photoacoustics, and Acoustical Phase Conjugation

12 PERSONAL AUTHOR(S)
Marston, P. L.

13a TYPE OF REPORT Annual Summary	13b TIME COVERED FROM 861001 TO 870915	14. DATE OF REPORT (Year, Month, Day) 1987 Sept. 15	15 PAGE COUNT 84

16 SUPPLEMENTARY NOTATION
The telephone number for the Principal Investigator, P. L. Marston, is (509) 335-5343 or 335-9531.

17	COSATI CODES		18 SUBJECT TERMS (Continue on reverse if necessary and identify by block number)
FIELD	GROUP	SUB-GROUP	Acoustical Scattering, Lamb Waves, Resonances, Diffraction Catastrophes, Caustics, Light Scattering, Microbubbles, Bubbles, Photoacoustics, Phase Conjugation (Acoustical).

19 ABSTRACT (Continue on reverse if necessary and identify by block number)

⟹ The research summarized concerns several aspects of the propagation and scattering of acoustical and optical waves. The topics discussed fall under the following five categories:

→ A. Acoustical scattering theory and experiments for elastic objects in water (the coupling of sound with surface waves on fluid loaded elastic objects as →

20 DISTRIBUTION/AVAILABILITY OF ABSTRACT ☒ UNCLASSIFIED/UNLIMITED ☐ SAME AS RPT ☐ DTIC USERS	21 ABSTRACT SECURITY CLASSIFICATION Unclassified
22a NAME OF RESPONSIBLE INDIVIDUAL L. E. Hargrove	22b TELEPHONE (Include Area Code) (202) 696-4221	22c OFFICE SYMBOL ONR Code 1112

DD Form 1473, JUN 86   Previous editions are obsolete.   SECURITY CLASSIFICATION OF THIS PAGE

UNCLASSIFIED

19. ABSTRACT (continued)

described by a generalization of GTD, confirmation from measurements of focused backscattering due to Lamb waves on a spherical shell);

B. Light scattering from real bubbles and microbubbles in water (the unfolded glory or backscattering pattern of an oblate bubble in water, observation of Brewster angle scattering of polarized light and the effects of adsorbed films which may coat the bubble);

C. Production of sound by a drop or bubble in water illuminated by modulated laser light and the optical levitation of bubbles;

D. Acoustical and optical diffraction catastrophes (theory and optical simulation of transverse cusps, experiments with acoustical transverse cusps produced by reflection from smooth surfaces and the merging of echoes at caustics, the wavefield in a hyperbolic umbilic focal section, applications to the theory of shock wave focusing);

E. Acoustical phase conjugation (theory of the focal-point shift for the reversed wave resulting from three-wave mixing in a bubble layer, experimental evidence for the existence of such a wave).

REPORT NUMBER N00014-85-C-01410AR7

DEPARTMENT OF PHYSICS

WASHINGTON STATE UNIVERSITY

PULLMAN, WA   99164-2814

ANNUAL SUMMARY REPORT NO. 7

SEPTEMBER, 1987

Title:

Research on Acoustical Scattering, Diffraction Catastrophes, Optics of

Bubbles, Photoacoustics, and Acoustical Phase Conjugation

by

Philip L. Marston

Prepared for:

OFFICE OF NAVAL RESEARCH

PHYSICS DIVISION—CODE 1112

CONTRACT NO. N00014-85-C-0141

Accesion For		
NTIS CRA&I	☑	
DTIC TAB	☐	
Unannounced	☐	
Justification		
By		
Distribution /		
Availability Codes		
Dist	Avail and / or Special	
A-1		

DTIC COPY INSPECTED 6

87 10 21 005

ABSTRACT

The research summarized concerns several aspects of the propagation and scattering of acoustical and optical waves. The topics discussed fall under the following five categories:

A. Acoustical scattering theory and experiments for elastic objects in water (the coupling of sound with surface waves on fluid loaded elastic objects as described by a generalization of GTD, confirmation from measurements of focused backscattering due to Lamb waves on a spherical shell);

B. Light scattering from real bubbles and microbubbles in water (the unfolded glory or backscattering pattern of an oblate bubble in water, observation of Brewster angle scattering of polarized light and the effects of adsorbed films which may coat the bubble);

C. Production of sound by a drop or bubble in water illuminated by modulated laser light and the optical levitation of bubbles;

D. Acoustical and optical diffraction catastrophes (theory and optical simulation of transverse cusps, experiments with acoustical transverse cusps produced by reflection from smooth surfaces and the merging of echoes at caustics, the wavefield in a hyperbolic umbilic focal section, applications to the theory of shock wave focusing);

E. Acoustical phase conjugation (theory of the focal-point shift for the reversed wave resulting from three-wave mixing in a bubble layer, experimental evidence for the existence of such a wave).

TABLE OF CONTENTS

Page

I. EXTERNAL COMMUNICATIONS SUPPORTED BY THIS CONTRACT (since October 1, 1986):

A. Papers Published in Refereed Journals:

1. P. L. Marston, "Transverse cusp diffraction catastrophes: some pertinent wavefronts and a Pearcey approximation to the wavefield," Journal of the Acoustical Society of America 81, 226-232 (1987).

2. P. L. Marston, "Review of the book Wave Propagation and Scattering edited by B. J. Uscinski," Journal of the Acoustical Society of America 82, 401 (1987).

B. Papers Submitted to Refereed Journals:

1. P. L. Marston, "GTD for backscattering from elastic spheres and cylinders in water, resonances, and the coupling of surface elastic waves with the acoustic field," J. Acoust. Soc. Am. (submitted March 1987).

2. W. P. Arnott and P. L. Marston, "Optical glory of small freely-rising gas bubbles in water: Observed and computed cross-polarized backscattering patterns," J. Opt. Soc. Am. A (submitted July 1987).

3. B. T. Unger and P. L. Marston, "Optical levitation of bubbles in water by the radiation pressure of a laser beam: an acoustically quiet levitator," J. Acoust. Soc. Am. (submitted July 1987).

C. Books (and sections thereof) Published: (Note—these items were typically subject to review by committee or by a topical editor):

1. D. S. Langley and P. L. Marston, "Forward optical glory of bubbles: Theory and Observations," in Proceedings of the 1985 Scientific

Conference on Obscuration and Aerosol Research, edited by R. H.
Kohl (Chemical Research Development and Engineering Center,
Aberdeen Proving Ground, MD, 1986) pp. 411-412.

2. P. L. Marston and E. H. Trinh, "Diffraction catastrophes and inverse
    scattering from spheroidal drops," in same proceedings as the
    preceding item, pp. 439-440.

3. P. L. Marston and D. S. Langley, "Forward optical glory from bubbles
    (and clouds of bubbles) in liquids and other novel directional caustics,"
    in Multiple Scattering of Waves in Random Media and Random Rough
    Surfaces, edited by V. V. Varadan and V. K. Varadan (Pennsylvania
    State University, University Park, PA, 1987) pp. 419-429.

D. Books (and sections thereof) Submitted for Publication:

1. P. L. Marston, "Surface shapes giving transverse cusp catastrophes in
    acoustic or seismic echoes," for Acoustical Imaging Vol. 16
    [Proceedings of the 16th International Symposium on Acoustical
    Imaging, Chicago, June, 1987] edited by L. W. Kessler (Plenum, to
    be published).

2. P. L. Marston, "Wavefront Geometries Giving Transverse Cusp and
    Hyperbolic Umbilic Foci in Acoustic Shocks," for the Proceedings of
    the APS 1987 Topical Conference on Shock Waves in Condensed
    Matter, Monterey, California, 20-23 July, 1987, edited by S. C.
    Schmidt and N. C. Holmes (North Holland Publishing, to be
    published).

E. **Invited** Presentations at Topical or Scientific/Technical Society Conferences:

    1. None.

F. **Abstracts of Papers (presented at meetings) Containing Significant Information Not Yet Published (or submitted for publication) in Final Form:**

    1. S. C. Billette and P. L. Marston, "Scattering of light by a coated bubble in water near the critical scattering angle," J. Opt. Soc. Am. A 3 (13), 117 (1986).

    2. W. P. Arnott and P. L. Marston, "Backscattering from a slightly spheroidal air bubble in water: A novel unfolding of the optical glory," J. Opt. Soc. Am. A 3 (13) 117 (1986).

    3. P. L. Marston, "Hyperbolic-umbilic diffraction catastrophes and the tracing of local principal curvatures of wavefronts," J. Acoust. Soc. Am. Suppl. 80, 73 (1986).

    4. W. P. Arnott and P. L. Marston, "Backscattering of light from spherical and slightly spheroidal air bubbles in water: A novel unfolding of the glory," J. Acoust. Soc. Am. Suppl. 80, 73 (1986).

    5. P. L. Marston and S. C. Billette, "Scattering of light by a coated bubble in water near the critical and Brewster scattering angles" J. Acoust. Soc. Am. Suppl. 80, 59 (1986).

    6. P. L. Marston, "Coupling coefficient G for the Fabry-Perot representation of backscattering from spheres and cylinders:

Quantitative GTD for elastic objects in water," J. Acoust. Soc. Am. Suppl. $\underline{81}$, 14 (1987).

7. P. L. Marston, "Hyperbolic-umbilic focal sections: The wavefield and the merging of rays at caustic lines," J. Acoust. Soc. Am. Suppl. $\underline{81}$, 14 (1987).

8. S. G. Kargl and P. L. Marston, "Focused backscattering from hollow spherical shells in water: Lamb waves and the acoustical glory," J. Acoust. Soc. Am. Suppl. $\underline{81}$, 14 (1987).

G. Reports Issued:

1. P. L. Marston, <u>Annual Summary Report No. 6, Research on Acoustical Scattering, Diffraction Catastrophes, Optics of Bubbles, Photoacoustics, and Acoustical Phase Conjugation</u>, issued October 1986 (available from the Defense Technical Information Center, Cameron Station, Alexandria, VA, Accession No. AD-A174401) 48 pages.

2. S. C. Billette and P. L. Marston, "Computational Analysis of the Effects of Surface Films on the Optical Scattering Properties of Bubbles in Water," <u>Technical Report</u> issued under contracts N00014-85-C-0141 and N00014-86-K-0242 (October, 1986), Accession Number AD-A173992 (Defense Technical Information Center, Alexandria, VA) 166 pages.

H. Dissertations Supported in Part by This Contract:

1. Bruce T. Unger, "Optically Stimulated Sound from Gas Bubbles in Water" (Department of Physics, Ph.D. Dissertation, Washington State University, May 1987).

2. Steven G. Kargl, "Focused Backscattering of Lamb Waves from Elastic Spherical Shells in Water," M.S. Project paper, July, 1987. (Note: This was not a formal thesis since none was required. This paper was thesis quality.)

II. PREFACE; EXPLANATION OF CITATION SYSTEM USED FOR REFERENCES; AND LIST OF GRADUATE STUDENTS SUPPORTED

This report summarizes progress in research supported by the contract titled: "Propagation and Effects of Acoustical and Optical Waves." The emphasis of the report is on progress subsequent to that described in the previous Annual Summary Report, item G1 in the preceding list of "External Communications." However, for continuity, certain research items discussed there will also be mentioned. The principal sections (indicated by different Roman numerals) may be read independently of each other.

The following reference system is used in this report. References to recent external communications supported by this contract will be made by giving the section letter and number of the list given in Sec. I of the present report. For example, the first item listed in Sec. I is referenced as [A1]. Reference to other literature, including earlier work supported by this contract, are listed in Sec. IX. The first item in that list is referenced as [1].

The following students were supported either entirely or in part by the contract during the period October 1, 1986 - September 30, 1987.

1. William Pat Arnott
2. Steven G. Kargl
3. Cleon E. Dean
4. Carl K. Frederickson

In addition, the following former student was supported on a part-time basis for work towards the completion of manuscripts[B3] and other contract related tasks.[B1]

1. Bruce T. Unger

III. ACOUSTICAL SCATTERING THEORY AND EXPERIMENTS

A. Motivation for this Research: An Overview.

The general motivation for research into acoustic scattering from elastic objects of simple shape has been discussed previously.[1-3] The present work[B1,F6,F8,H2] emphasizes the generalization of the geometrical theory of diffraction (GTD) so as to give quantitative predictions of surface elastic wave (SEW) contributions to the scattering from spheres based on simple expressions. It may be thought that scattering from elastic spheres is too specialized of a problem to be of any practical consequence; however, we intend to show that our quantitative modeling of the surface-wave contributions to scattering, which we have studied for spheres, is helpful for understanding the echoes from complicated elastic structures. The experiments on the backscattering of sound from elastic hemispheres in water (described in Ref. G1) were a step in that direction. The previous work on the quantitative prediction of surface wave contributions to the scattering from elastic spheres was concerned with solid spheres[3-5] whereas the emphasis of the current experiments is on hollow (air-filled) elastic spheres. In all cases the surrounding medium is water.

One important aspect of our research is our ability to model and measure scattering amplitudes not just in the exact backward direction but also in near backward directions since the width of the diffraction lobes in near-backward directions are indicative of the target's size.[3]

B. Coupling of Sound with Surface Waves on Fluid-Loaded Elastic Objects Described by a Generalization of GTD.

The geometrical theory of diffraction (GTD) was recently extended to describe surface elastic wave (SEW) contributions to scattering from fluid-loaded spheres and cylinders at high frequencies.[B1,F6] The coupling of a SEW with the acoustic field was described by a complex "coupling" coefficient G_l. The original introduction of G_l into the description of scattering was through the application of the Sommerfeld-Watson Transformation (SWT) to the partial-wave series for the scattering from a solid elastic sphere.[4,5] (Since that work was funded through the present contract it is reviewed in the previous Annual Reports.[3,G1]) For the purposes of the present discussion we need only note the form of the equations given by the SWT. Consider first the case of an incident tone burst which is sufficiently short that the SWT echoes do not overlap but sufficiently long that a narrow-band calculation for the SEW parameters can be used. (The calculation of the SEW parameters assumes a single frequency and hence a single size parameter ka, a = sphere radius, $k = 2\pi/$wavelength in water.) This turns out to be an accurate assumption for the experiments described below in Sec. IIIB. Let $|p_i|$ denote the pressure amplitude of the incident tone burst and let $|p_m|$ denote the amplitude of the m echo for a given class l of SEW echo. The SWT gives $|p_m| = |p_i| A_{ml} a/2r$; r is the distance from the center of the sphere and[3,4]

$$A_{ml} = |G_l| e^{-2(\pi - \theta_l)\beta_l} e^{-2\pi m \beta_l}, \tag{1}$$

where the earliest SEW echo is designated by $m = 0$ and subsequent echoes by $m = 1$, 2, ...

The parameter β_l specifies the value of the radiation damping for the l class of SEW at the frequency specified by ka. Let c_l and c denote the phase velocities for the SEW and the acoustic waves in the water. The angle $\theta_l = \sin^{-1}(c/c_l)$ has the significance

of being the local angle of incidence where the incident wave and the SEW are coupled. The important point here is that while both β_l and c_l (and hence θ_l) are relatively easy to calculate for Eq. (1), the full expression for G_l is difficult to interpret physically and has been evaluated only through numerical differentiation on a computer.[4] Furthermore, the exact expression for G_l for the case of a hollow sphere (see Sec. IIIC), has yet to be found. Hence the derivation of a simple physical approximation to G_l was justified.

The SWT also gives the following expression for the contribution to the form function f for the case of steady-state backscattering[5]

$$ f_l = \frac{-G_l\, e^{-2(\pi-\theta_l)\beta_l}\, e^{i\eta_l}}{\left[1 + j\exp(-2\pi\beta_l + i2\pi xc/c_l)\right]} \tag{2} $$

where $x \equiv ka$ and for the present problem of spheres $j = +1$ and η_l is a propagation related phase shift which has a simple physical form. The expression Eq. (2) may be referred to as a Fabry-Perot representation for the amplitude since the denominator is formally like the one which appears in the analysis of Fabry-Perot resonators. The exact SWT result for G_l was used to show[5,G1] that a superposition of a specular reflection with various f_l can give an accurate approximation of the total $|f|$ for solid spheres for ka as small as 10. No Franz wave ("creeping wave") contribution was needed to obtain an accurate synthesis.

The new analysis gives the following simple approximation for the case of a spherical scatterer[B1,F6]

$$ G_l \approx G_l^{sp}, \qquad \left|G_l^{sp}(x)\right| = 8\pi\beta_l\, c/c_l . \tag{3a,b} $$

The correctness of this approximation was confirmed by comparing $|G_l^{sp}(x)|$ with $|G_l(x)|$ as given by the SWT for two different classes of SEW and two different sphere materials in water.

The comparison is shown in Figs. 1 and 2. It is noteworthy that the approximation Eq. (3) is more accurate than might have been anticipated from the derivation which was based on a comparison of Eq. (2) with the local resonance form given by Resonance Scattering Theory. It is noteworthy that the proportionality of G_l^{sp} on β_l and c/c_l can be argued from GTD-based concepts.

Note that the phase of G_l^{sp} is not specified by Eq. (3). The numerical calculations of the phase of G_l suggest that it is an accurate approximation to take[B1]

$$\arg G_l^{sp} = 0. \qquad (4)$$

The usefulness of the resulting approximation $G_l \approx 8\pi\beta_l \, c/c_l$ has been confirmed by Dr. Kevin L. Williams of the Naval Coastal Systems Center. Williams found that if this approximation is used in Eq. (2), the resulting synthesis of |f| is in good agreement with both the exact |f| and the synthesis based directly on the SWT for the specific case tried[6] (tungsten carbide in water).

For the case of a Rayleigh wave, at large values of ka the following approximation for the radiation damping coefficient is useful[B1]

$$\beta_R(ka) \approx ka \, \beta_R'(\infty), \qquad (5)$$

where the factor $\beta_R'(\infty)$ may be calculated from an approximation[B1] which does not require the solution of transcendental equations. The energy conservation method used to obtain $\beta_R'(\infty)$ is known to be applicable to cases where the substrate has anisotropic elastic properties and for other SEW types in addition to Rayleigh waves.

Consider now the steady state backscattering of a plane wave from a circular cylinder of radius a. The pressure p_{scat} at a distance r from the center of a cylinder of radius a is

$$p_{scat} = (a/2r)^{1/2} \, p_i f \, e^{i(kr-\omega t)}, \qquad (6)$$
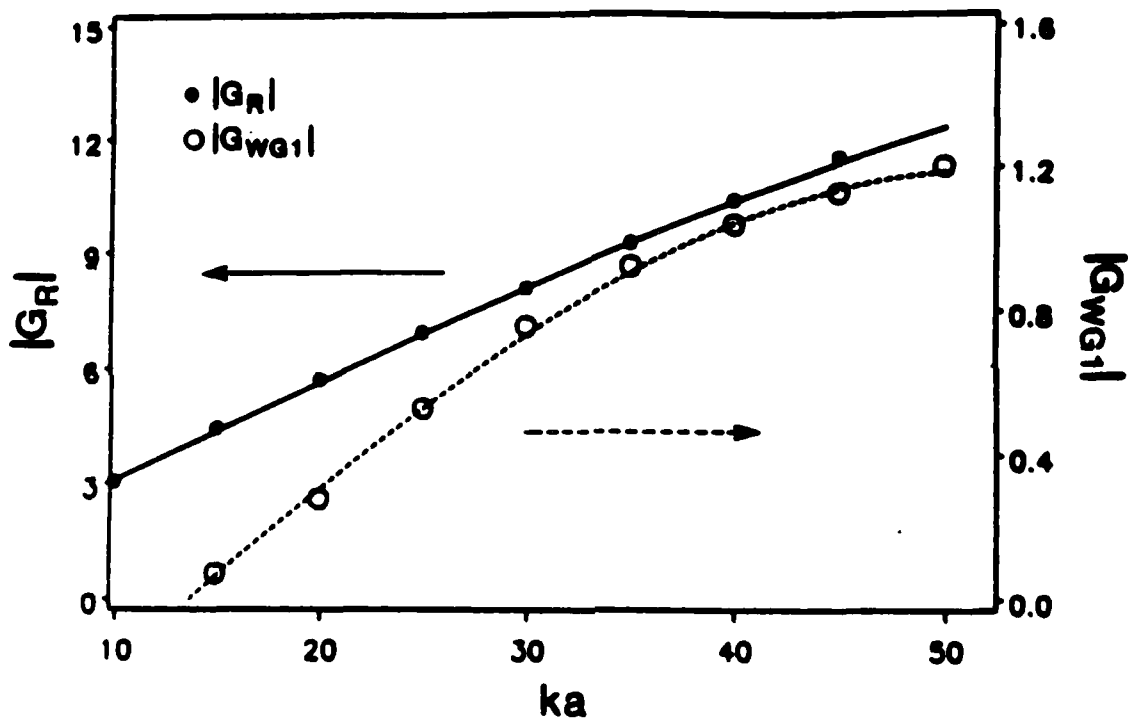
Fig. 1. The modulus of the coupling coefficient G_l for the Rayleigh and slowest whispering gallery waves for an aluminum sphere in water. For each class of wave, $|G_l|$ was obtained by two different methods. The points are from numerical evaluation of the direct result of the Sommerfeld Watson transformation. The corresponding curves are from the simple approximation given as Eq. (3b). The low end of the plotted ka range was set to avoid possible numerical inaccuracy (see Ref. 5). It does not necessarily indicate the lowest ka where Eq. (3b) is applicable.
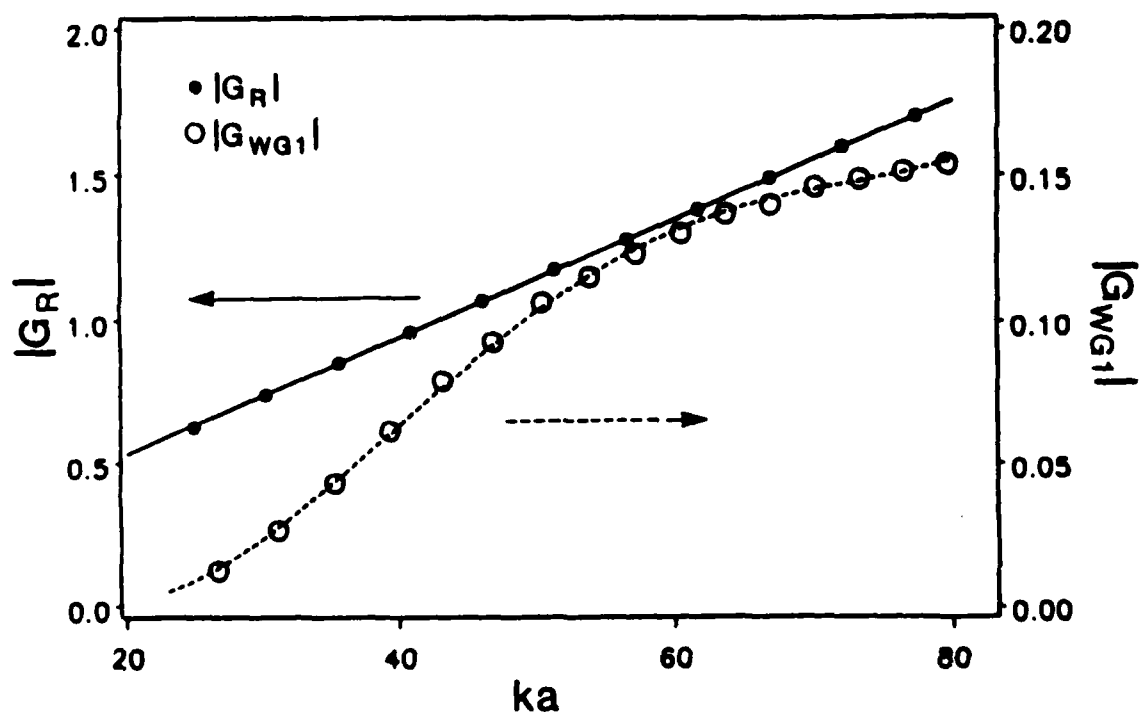
Fig. 2. Like Fig. 1 but for a tungsten carbide sphere in water.

where f is the complex form function. For the lth class of SEW the contribution to f has a Fabry-Perot representation given by Eq. (2) with[B1] $j = -1$. The difficulty in applying this result is that an exact expression for G_l in the case of cylinders is not known. The method of approximation leading to Eq. (3) was repeated for cylinders with the result

$$G_l \sim G_l^{cy}, \quad |G_l^{cy}(x)| = 8\pi\beta/(\pi x)^{1/2}, \tag{7a,b}$$

where $x = ka$. For a specific case of a Lamb wave on a hollow cylindrical shell in water, numerical data are available which indicate that Eq. (7) is an accurate approximation. The ratio $|G_l^{sp}/G_l^{cy}|$ may be derived independently from GTD-based arguments.[B1]

C. Focused Backscattering of Sound from Elastic Spherical Shells in Water Due to Lamb Waves on the Shell (S. Kargl)

This work is the research project of Steve Kargl which was used towards the fulfillment of the requirements of an M.S. Degree in Physics.[H2] The ray diagram for the Lamb wave contributions to the backscattering from a hollow shell is shown in Fig. 3. In the experiments, the sound wave incident on the sphere was a tone burst having a duration of 4 cycles. Representative records for backscattering are shown in Fig. 4. The record in Fig. 4(i) is the case of a solid tungsten carbide sphere in water. The Rayleigh echo amplitudes are known[4] to be described by Eq. (1). The other records, Fig. 4(ii), (iii), and (iv) are for a hollow stainless steel sphere having an outer radius $a = 1.905$ cm and an inner radius b with $b/a = 0.84$. Two types of SEW echoes were identified for the hollow sphere. These are the echoes associated with the first antisymmetric Lamb wave (denoted by A) and the first symmetric Lamb wave (denoted by S). The antisymmetric wave is a flexural wave while the symmetric wave is essentially a dilatational wave. The time delays of the SEW echoes relative to the leading edge of the specular reflection have been measured for ka from 24 to 75 and are in good agreement with the GTD based theory.
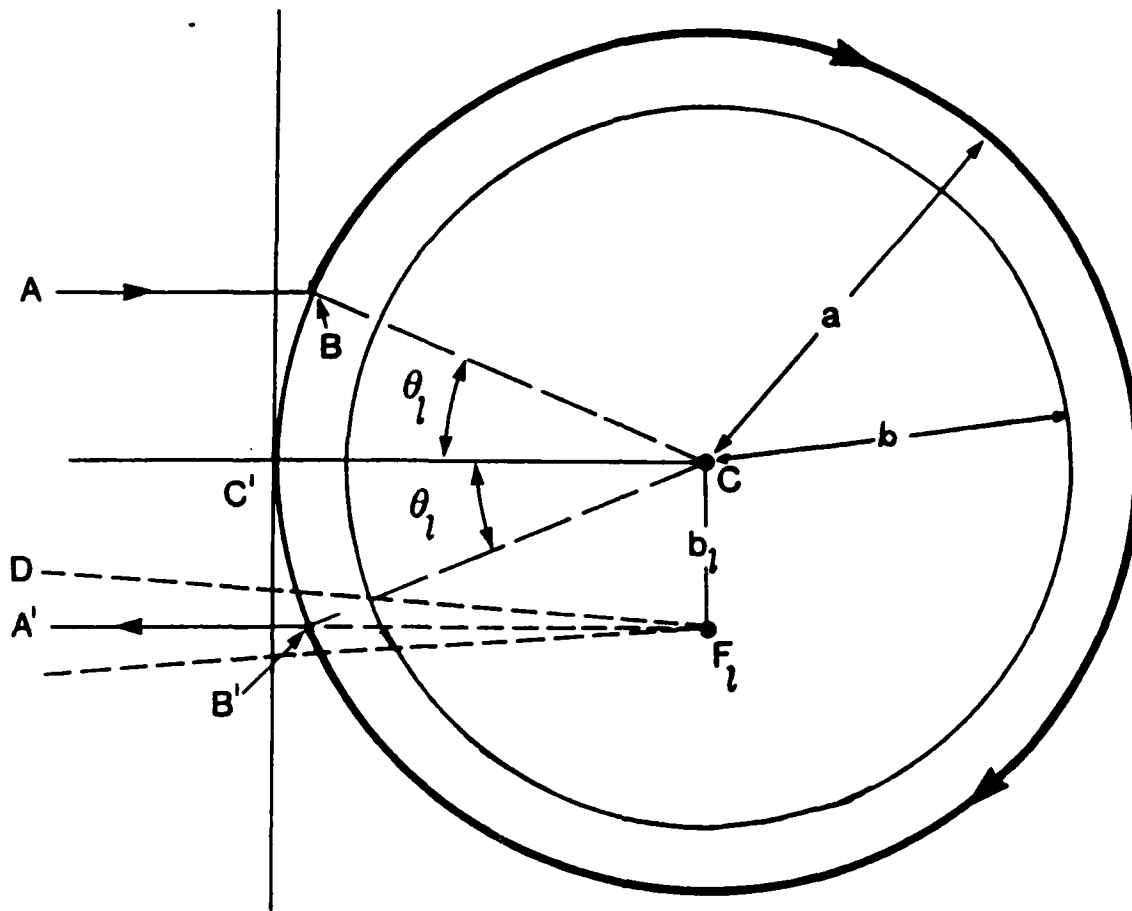
Fig. 3. The diagram demonstrates the "ray" acoustic analysis of the Lamb waves on an elastic shell. The point C' is the point of tangency of an incident plane wavefront with the shell. The point B is the location for coupling the Lamb wave acoustic field to the shell and point B' is the radiation point for backscattering. The angle θ_l is determined by the phase velocity trace matching condition. The radius b_l is the location where a virtual ring-like source cuts the plane of the page at F_l. The ray A'B' is the "glory ray" and the ray DF_l is the ray that is focused on-axis at the detector.
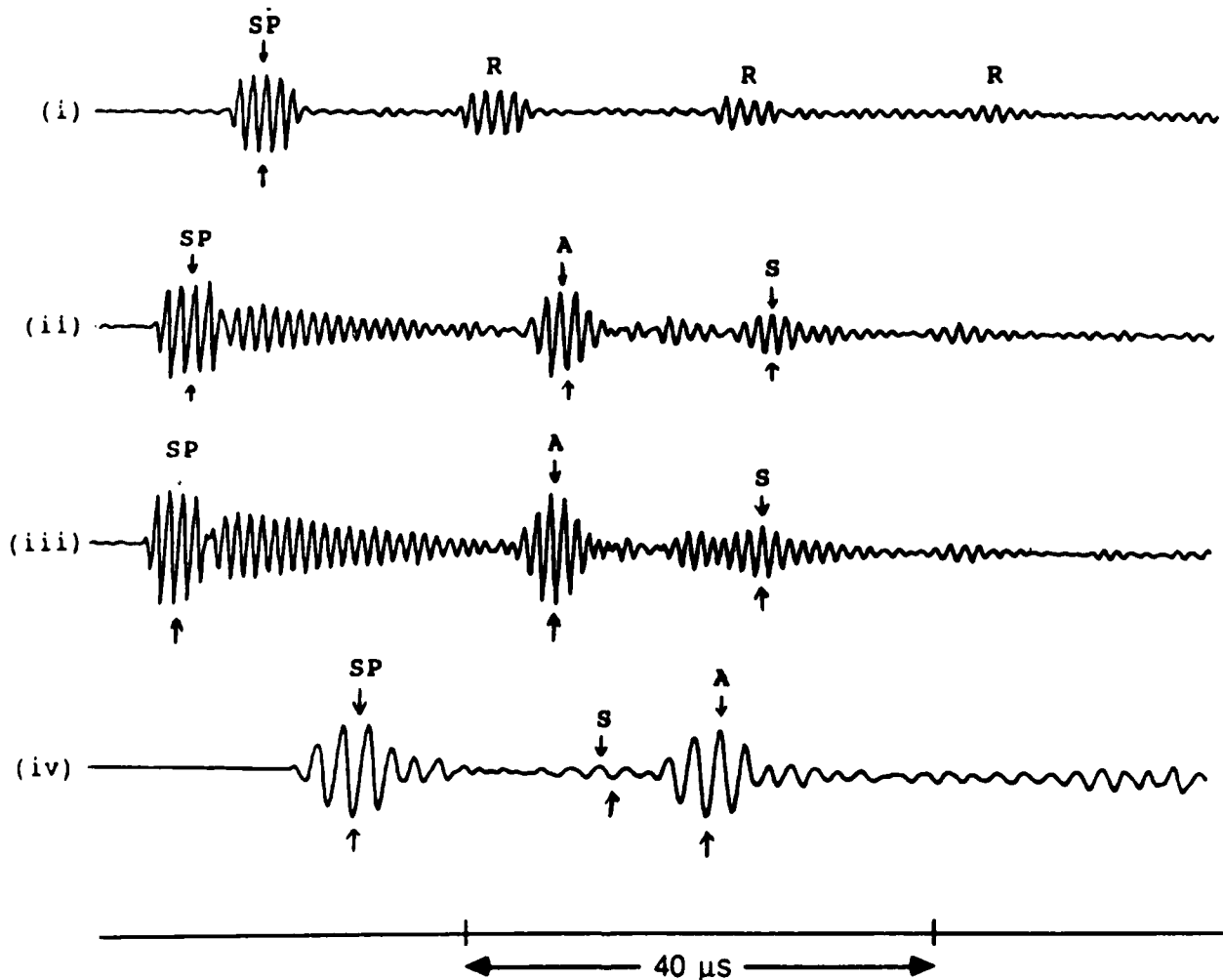
Fig. 4. The backscattering for (i) solid tungsten carbide sphere, (ii) 440C stainless steel shell at a frequency f = 0.80 MHz, (iii) 440C stainless steel shell at f = 0.85 MHz, and (iv) 440C stainless steel shell at f = 0.45 MHz. The specular reflections, Rayleigh surface wave echoes, first antisymmetric (flexural) Lamb wave and first symmetric (dilatational) Lamb wave are denoted by SP, R, A, and S respectively. The arrows designate the positions of peak-to-peak voltage measurements.

Before considering the amplitudes of the various SEW echoes, it is appropriate to note a novel feature of the specular echoes in Fig. 4(ii) and (iii). In those cases a long ringing tail follows the relatively square topped specular echo. This tail appears to be a consequence of the reverberation of a bulk longitudinal wave within the shell. The shell thickness is 3.1 mm so that the round-trip transit time of such a wave is only 6.2 mm/5.85 mm/μs = 1.06 μs. The frequency of the lowest resonance of such a thickness mode for the shell should be approximately $(1.06 \, \mu s)^{-1} = 0.95$ MHz. The experiments showed the ringing was most pronounced when the frequency of the burst was in the range 0.85 to 0.95 MHz which supports the idea that it results from a thickness (longitudinal) mode of a plate which has been curved into the form of a shell.

Let us return now to the central problem of interest, the amplitudes of the Lamb wave echoes for backscattering labeled A and S in Fig. 4. It is convenient to express echo amplitudes for the mth echo of the lth class of SEW with the following normalization (see above Eq. (1)):

$$A_{ml} = \frac{|p_m|}{|p_i|} \frac{2r}{a} \, , \tag{8}$$

where $|p_m|$ is the echo amplitude, r is the distance to the hydrophone, and a is the sphere radius. In the experiments, the quantities A_{ml} are for $m = 0$ and $l = S$ or A. Calibration was achieved by comparison with the specular echo amplitude from a tungsten carbide sphere.[H2] The resulting measured normalized amplitudes A_{0l} over a range of ka are shown in Fig. 5. Figure 5 also shows curves (the small points) which are given by evaluating Eq. (1) with $|G_l|$ given by Marston's approximation, Eq. (3). It is important to note that there is presently no exact theory available for calculating G_l in the case of a hollow sphere. In the region of ka from 45 to 55 the meaning of the measurements is not clear since the echoes due to the symmetric and antisymmetric Lamb waves overlap in time. Outside this region the agreement is satisfactory. At large ka, the variation in the data for
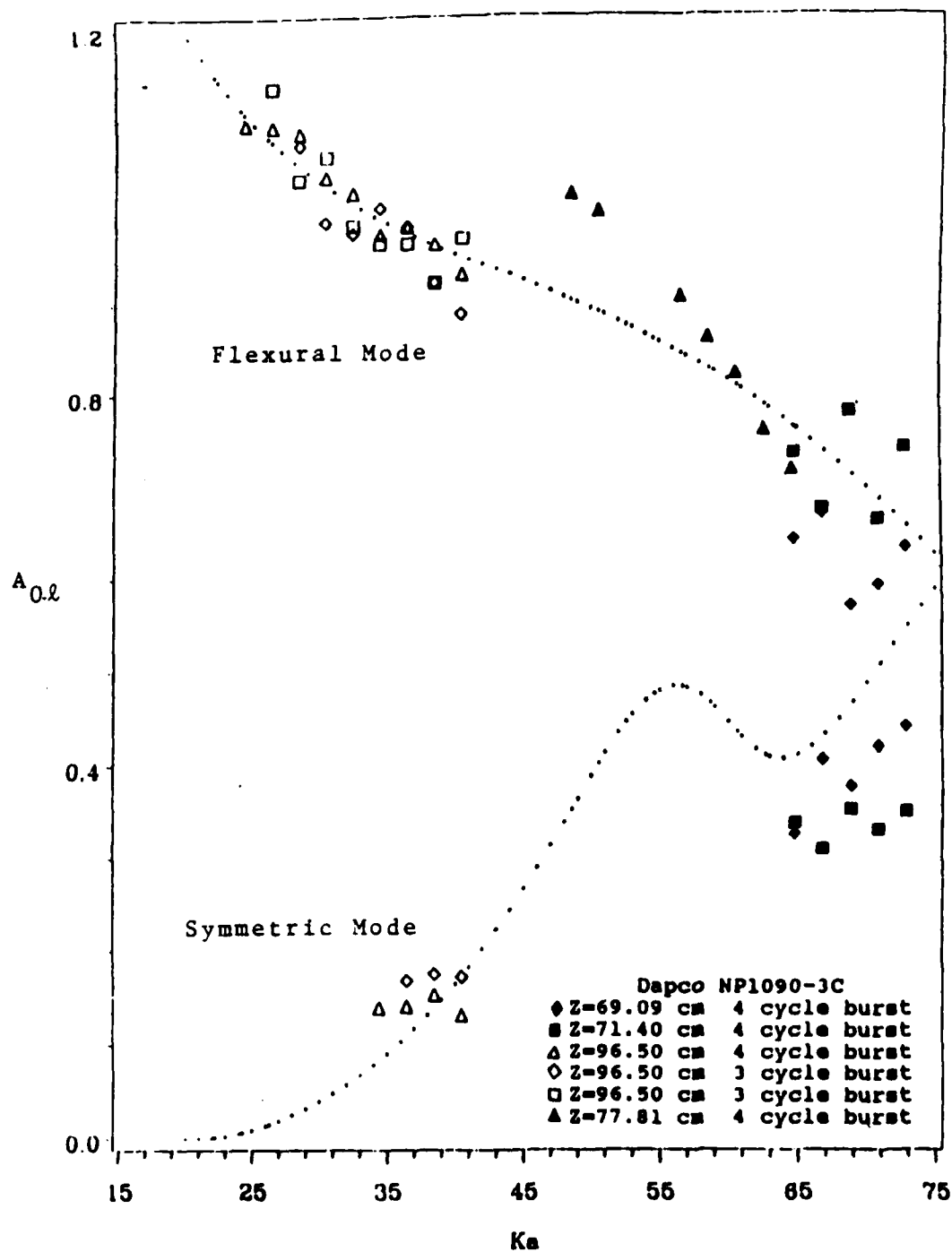
Fig. 5. The theoretical normalized backscattered amplitudes (dotted lines) for the first antisymmetric and symmetric Lamb waves are compared with experimental data. The upper curve (dots) corresponds to the theory for the first antisymmetric mode while the lower curve (dots) is for the first symmetric mode.. The low ka data are correctly predicted. The high frequency data may be affected by various experimental problems (see Kargl's "thesis," Ref. H2).
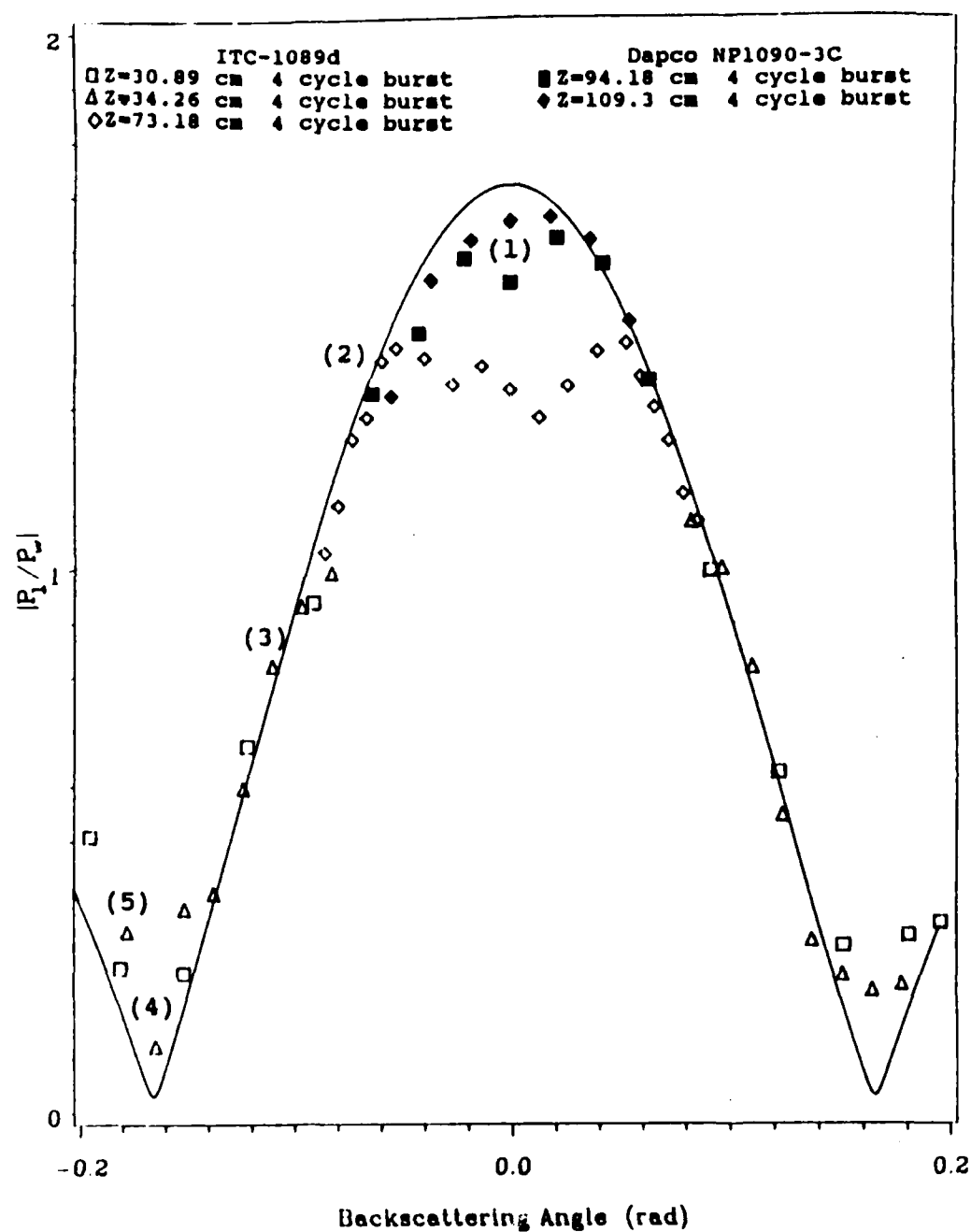
Fig. 6. The experimental confirmation of the axial focusing predicted by the theory. The solid curve is the theoretical result for ka = 24.3. The experimental data and theory agree in the vicinity of the maximum. Note the depression in the central region of the unshaded diamonds is associated with the use of the larger of the hydrophones.

the antisymmetric amplitude may be due to interference with the aforementioned tail from ringing which follows the specular echo (see Fig. 4(iii)).

Consider now the dependence of the echo amplitude for a given class of SEW on the backscattering angle γ. The physical reasoning leading to axial focusing for SEW echoes from solid spheres[7] also applies to Lamb waves on hollow spheres. Indeed, in the previous annual report,[G1] Lamb wave echoes were demonstrated to be axially focused; however, since $|G_l|$ was not known, complete quantitative predictions for the amplitude were not possible. Use of Eq. (3) made quantitative predictions possible. The solid curve gives the predicted echo amplitude for the earliest antisymmetric Lamb wave (i.e. the flexural wave). The sphere is the aforementioned hollow stainless steel sphere with $ka = 24.3$ and the normalization is relative to the specular reflection from a tungsten carbide sphere having a radius of 12.7 mm. The data are in good agreement with the theory except for the case (unshaded diamonds) where γ is small and the ITC hydrophone was used for the receiver. Because of the large size of the ITC hydrophone a portion of the incident wave is blocked by the hydrophone when γ is small and the echo amplitude is reduced. The agreement was good in the central region, however, when a smaller hydrophone was used (shaded symbols). There are no adjustable parameters in the model.

IV. LIGHT SCATTERING FROM BUBBLES IN WATER: EMPHASIS ON "REAL" VERSUS "IDEAL" BUBBLES

A. Motivation and Review

This contract has previously supported research towards understanding the scattering of light from bubbles in water. The general approach and some possible applications in acoustics were reviewed in a previous Annual Summary Report.[3] Until recently[G1,G2] the research emphasized the case of spherical bubbles having a gas-liquid interface free of adsorbed layers of molecules.

B. Observations and Theory of Optical Backscattering from Freely Rising Bubbles in Water: The Unfolded Glory of an Oblate Bubble (W. P. Arnott)

Previous work on this problem by a graduate student, W. P. Arnott, is reviewed in the previous Annual Summary Report.[G1] During the past year Arnott has made progress towards completing a Ph.D. dissertation on this (and a similar problem relating catastrophe theory to backscattering from a spheroidal bubble) through the following activities:

(1) Experiments and theory for spherical bubbles in water.—It was apparent that prior to writing up a description of the perturbation theory for backscattering of light from slightly spheroidal bubbles, it would be necessary to give a more complete description and experimental test of the physical optics model for backscattering from bubbles in water which are sufficiently small so as to remain spherical as they rise through water. It was found that the backscattering pattern is essentially that of a sphere for bubble diameters $D \lesssim 0.3$ mm. Additional data were obtained for scattering from small bubbles

in this size range and a novel method of inferring the bubble size from the details of the backscattering pattern was demonstrated. Arnott has prepared a manuscript which describes both the experiments and the detailed physical optics model and this has been submitted for publication.[B2] Figure 7 shows several backscattering patterns which both illustrate the phenomena studied and the mutual agreement of the observations with exact Mie theory as well as the physical optics model. These may be compared with the previous results for bubbles in oil.[8]

(2) Further development of the perturbation model for the backscattering of light from slightly spheroidal air bubbles rising in water.—As discussed in the previous Annual Summary Report,[G1] when the diameter of the bubble in water
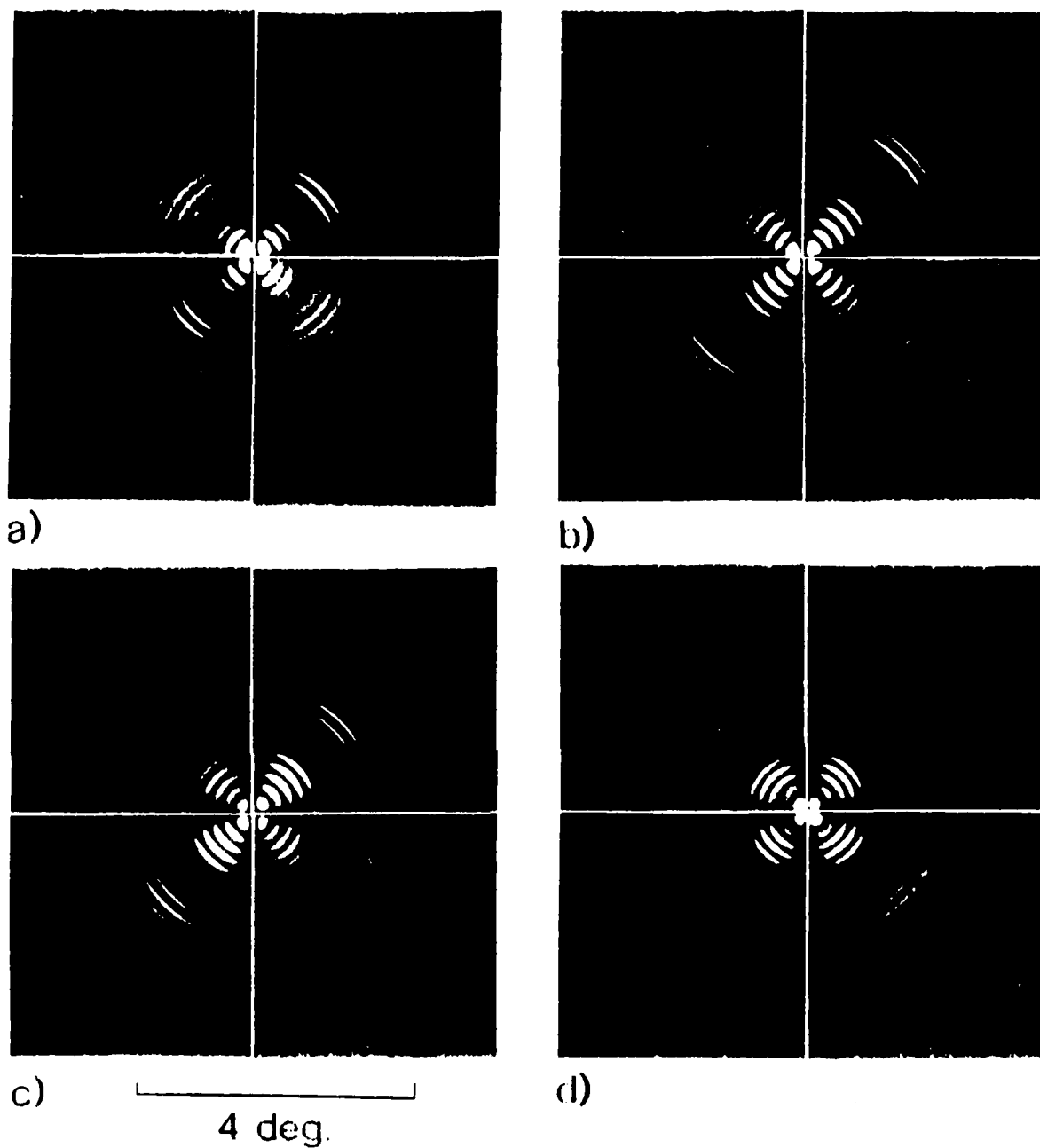
Fig. 7. Photographs of cross-polarized near backscattering by a freely rising bubble in water. The first and third quadrants of each composite pattern are computer-generated results from physical optics and Mie theory, respectively. White lines are borders of the synthesized patterns. In a, the experimentally measured radius was 123 μm, and best fit radius was 121.0 μm. In b and c, the radii were not measured and the best fit radii were 122.0 and 130.0 μm. In d, the experimentally measured radius was 140 μm while the best fit radius was 140.2 μm.

exceeds 0.3 mm, the symmetry of the scattering pattern changes. This evidently is a consequence of the oblate shape the bubble has in response to distribution of hydrodynamic stresses. A model was developed which starts with the physical optics model for spheres and correctly accounts for a small amount of oblateness.[F2,F4] The model adequately matches observed patterns for bubble diameter $D \lesssim 0.4$ mm. During the present contract period Arnott has made improvements to the model.

(3) Unfolding of the axial caustic for moderately oblate bubbles.—For bubbles having diameters $D > 0.5$ mm, the observed backscattering patterns were qualitatively different than those predicted by the perturbation theory since the theory assumed the oblateness of the bubble is finite but small. A different approach has been developed to facilitate an understanding of these patterns. Recall that for a spherical bubble the far-field caustic corresponds to a point in a given direction. The actual scattering pattern (see e.g., Fig. 7) corresponds to a diffraction pattern which is said to "decorate" the caustic. This pattern depends on polarization. Cross-polarized scattering is studied because it minimizes background noise.

Arnott has developed a model appropriate for larger bubbles which connects this work with the work Marston has been doing on transverse cusp diffraction catastrophes in optics[9] and acoustics.[A1] Specifically he has found that the axial directional caustic for backscattering from a sphere unfolds (in response to the broken symmetry of the spheroid) so as to produce a connected set of 4 transverse-cusp diffraction catastrophes. See Fig. 8. This is consistent with a conjecture by the British physicist M. V. Berry concerning the unfolding of axial caustics.[10] It is noteworthy that Arnott's analysis is clear as to the cause of these cusps and the results should be of general interest

Fig. 8. (see next page) Shape of the far-zone caustic for backscattering by an oblate bubble of equitorial diameter 585 μm. The experimental caustic in the lower figure is decorated by a spoked diffraction pattern. (Background noise was significant for this preliminary data.) In the lower figure, the calculated caustic outlines the experimental pattern. The axis scales are $(U,V) = (u/f, v/f)$ where f is the focal length of the camera lens and u,v are actual distances (horizontal and vertical) measured on the film negative.

V*1000

35.54

0.00

−35.54

−35.54　　　0.00　　　35.54

U*1000

V*1000

35.54

0.00

−35.54

−35.54　　　0.00　　　35.54
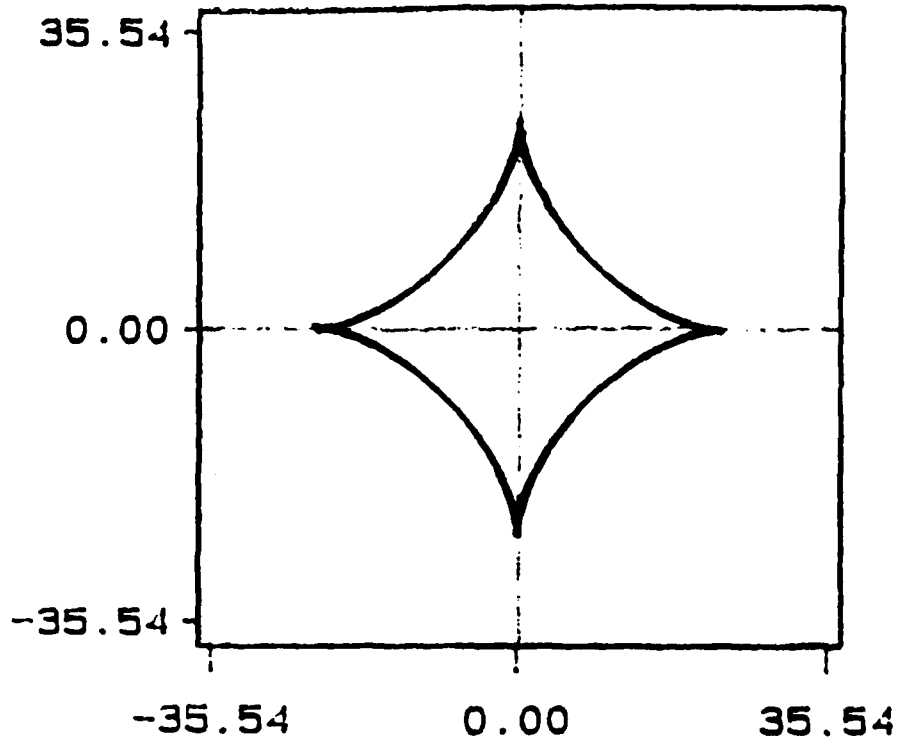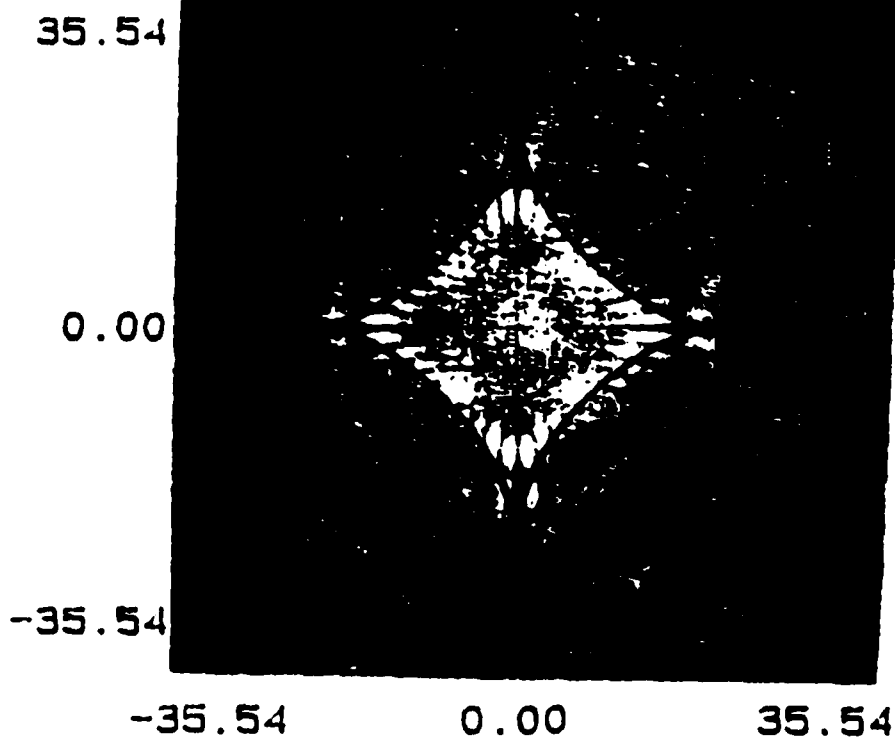
outside the specific application to backscattering from bubbles. The shape of the outgoing wavefront is as shown in Fig. 9 of the previous Annual Summary Report.[G1]

Figure 8 was computed for a bubble having a diameter of 0.585 mm. An off-set from the center of ± 35.54 units on the scale shown corresponds to a deviation from backscattering of ± 0.03554 radians ($\cong \pm 2.0$ degrees). The size of bubble used in the theory corresponds to the size (by direct measurement) of the bubble which produced the (cross-polarized) backscattering pattern also shown in Fig. 8 (lower part). The angle scale is the same as that for the theory so that figures may be overlayed. In agreement with the theory, the angular region inside (and adjacent to) the cusp curves appears bright.

(4) Other research by P. Arnott.—Arnott has assisted Marston and other students working on this project with numerous problems related to computer graphics. Arnott has also been working on applications of classical differential geometry to the tracing of wavefront (see Sec. VI).

C. Scattering of Light from a Coated Spherical Air Bubble in Water: A Computational Study of the Optical Effects of Adsorbed Films (C. E. Dean)

The motivation and general results on this problem are discussed in the previous Annual Summary Report[G1] and in a separate report.[G2,11] C. Dean began work on the present contract in autumn 1986 and was half supported by a recruitment fellowship (WSU funds). One of the first projects Dean worked on was to complete various computational tasks so that the work on scattering from coated bubbles done originally with S. Billette[F1,F5] (now with Hughes Aircraft) could be put in a form suitable for publication.

D. Observations of Brewster Angle Scattering from Freely-Rising Air Bubbles in Water (S. Bäumer)

For reasons noted below, Stefan Bäumer has been attempting photographic observations of the Brewster angle scattering from bubbles in water. Bäumer has been attending WSU with the support of a fellowship from his native country of West Germany. He requested the opportunity to work on an optics-related experiment for an M.S. thesis project. He has been carrying out experiments on a part-time basis since Autumn 1986 (but he was away during summer 1987). Though he has not been supported financially by contract funds, his laboratory supplies have been provided by contract resources since the objectives of his experiment are in line with those of proposed research.

To understand the motivation for Bäumer's experiments, it is helpful to review the reflective properties of a bubble in water.[12,G2] Consider first the geometric theory for polarized light reflected from the surface of an air bubble in water. The intensity of the reflected light corresponding to rays having a given angle of incidence at the bubble's surface, will depend on the local reflection coefficient. If the light is polarized parallel to the scattering plane, the flat surface reflection coefficient has a zero when the local angle of incidence is $i_B = 36.9$ deg for a water-to-air interface. The reflection from the curved bubble surface should be minimized near the corresponding "Brewster Scattering Angle" which is (180 deg - 2 i_B) = 106.2 deg. See Ref. 11, 12, and G2. Mie theory gives the exact scattered irradiance for an uncoated spherical bubble. The solid curve in Fig. 9 shows the scattered irradiance predicted for an uncoated bubble in water having a radius ≈ 0.061 mm = 61 μm for green light (here k_{light} a = 1000). The following features are evident in the region of the Brewster scattering angle (106.2 deg): (i) the contrast in the fine structure modulations is minimized near 106 deg; and (ii) the mean irradiance is small near that angle. The irradiance in this figure is normalized to that reflected from a perfectly reflecting sphere of the same size.

scattering angle (deg)
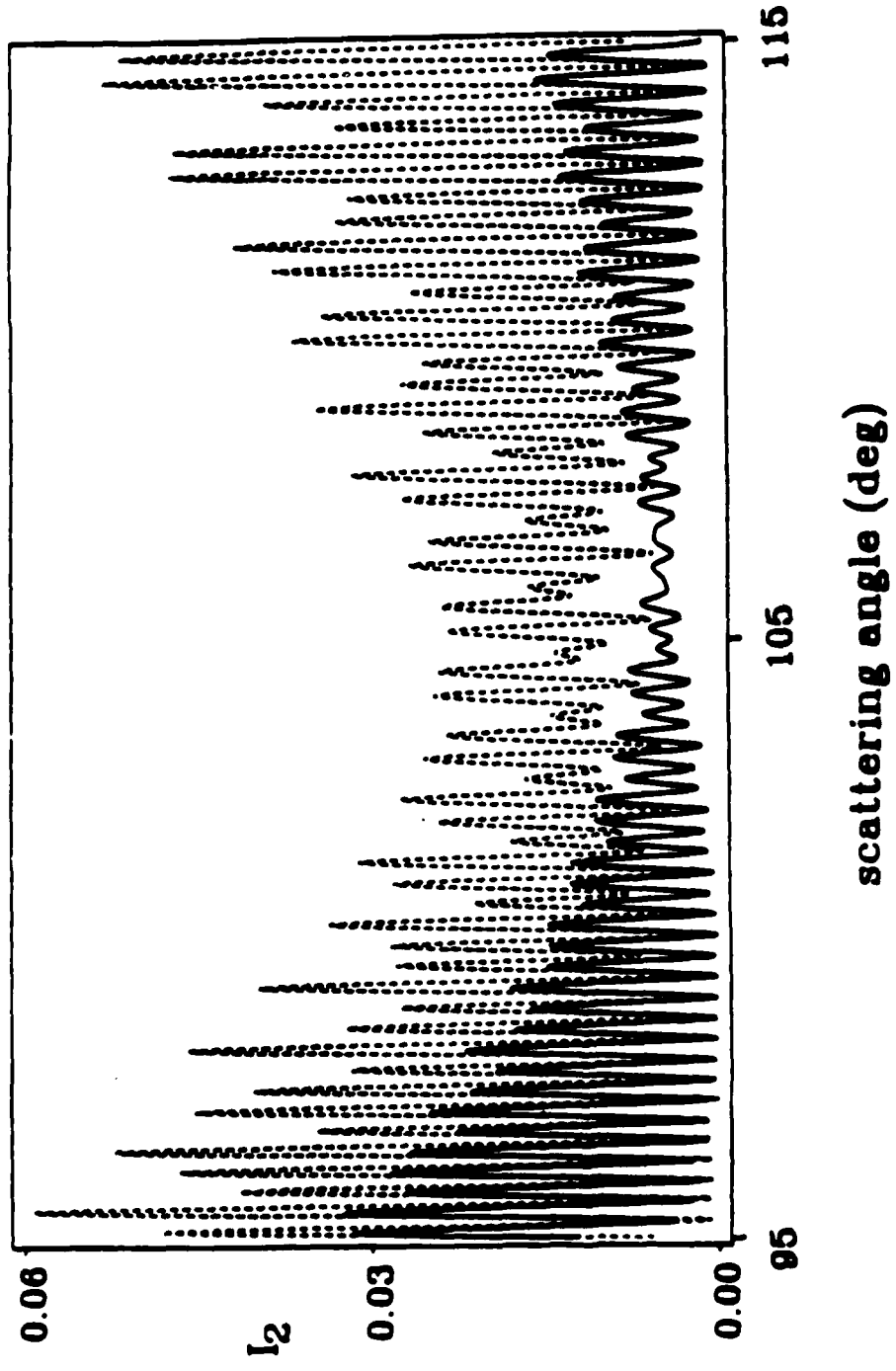
Fig. 9. The solid curve is the normalized scattered irradiance from a bubble in water for light polarized with the E field parallel to the scattering plane. It is given by Mie theory for $k_{light} a = 1000$. Note the structure near the Brewster scattering angle of 106 deg. The dashed curve is computed for an air bubble of the same size but having a coating (of a clear oil or other dielectric) at the air-water interface.
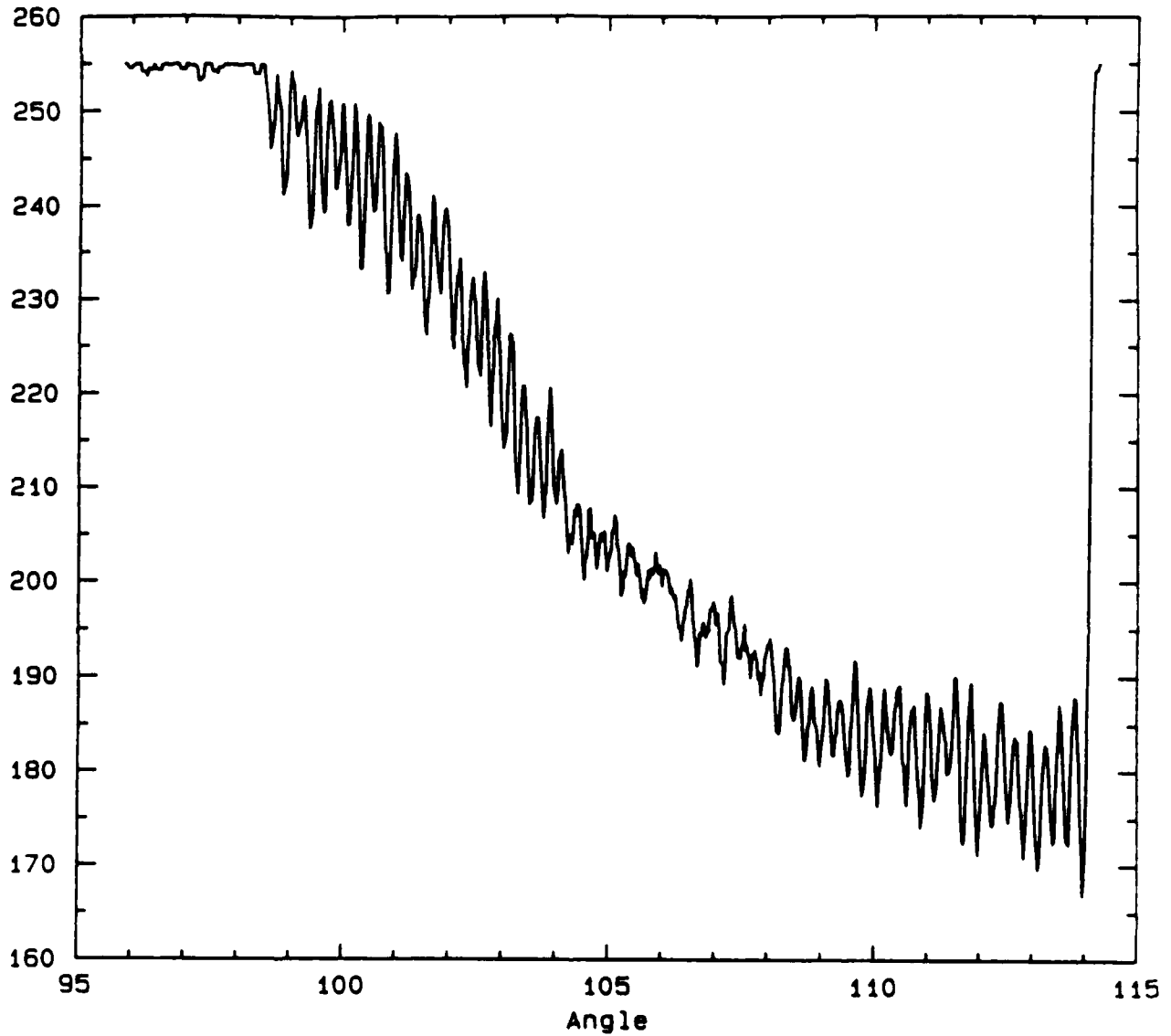
Fig. 10. Relative optical transmittance of a photographic negative which recorded the scattering pattern from a freely rising air bubble in water in the region of the Brewster scattering angle. In agreement with the solid curve of Fig. 9, the contrast in the fringe structure was minimized near 106 deg which suggests that the bubble did not have a significant coating.

Now consider the predictions shown in the dashed curve in Fig. 9. This curve was computed for a coated bubble by evaluating the appropriate partial-wave series.[11,G2] The coating thickness $h = 0.43$ μm (for green light) and refractive index $n_c = 1.50$ which is representative of an oily coating on the bubble. The radius of the gas pocket is the same as for the uncoated case (solid curve). Note that near 106 deg. there are two major changes relative to the uncoated case: (i) the contrast in the fine structure modulations is greatly enhanced, and (ii) the mean irradiance is shifted upwards.

From the discussion above, it is evident that observations of near Brewster angle scattering from freely rising air bubbles in water may provide a method for determining the thickness of an oily coating on the bubble. This is the motivation for Bäumer's observations though at present he has only examined the scattering from what are thought to be clean uncoated bubbles. The method for recording the scattering pattern is photography. Photographic negatives are scanned using the optical microdensitometer (of the WSU Shock Dynamics Laboratory). The "raw" form of the data is the optical transmittance of the negative as a function of position on the negative. Figure 10 shows a representative negative where the position on the negative has been converted to scattering angle. The bubble radius was 90 μm which is in the general range of sizes where features like those in Fig. 9 should be manifest. Inspection of Fig. 10 demonstrates one of the significant features of Brewster angle scattering: the contrast of the fringe structure is minimized near 106 deg. Unfortunately, the Brewster scattering features appear to be superposed on a smooth background (which appears not to be caused by scattering by the bubbles). One of Bäumer's next tasks is to minimize this background and to develop a method of subtracting it off so as to better display the features of Brewster angle scattering.

E. Optical Detection of Sound by Monitoring the Time Dependence of Light Scattered from Bubbles

The measurement of the time dependence of light scattered from bubbles was suggested as a method for the remote detection of sound by optical means.[1] During the present contract period, estimates have been done of the sensitivity of this method for the case where the acousto-optic coupling is through a shift in the fine structure near the critical scattering angle. Near that angle the scattering is strong and the fine structure is easy to detect.[13,G1,G2] The acquisition of a new 500 gallon water tank should make possible experiments for detecting the arrival of tone bursts (frequency ≈ 300 kHz) at a bubble by means of light scattering. Unfortunately this has not yet been possible since the tank has been used for other experiments (see Sec. VI and VII).

Some comments on the anticipated sensitivity are merited. Perhaps the simplest method of detecting sound by way of light scattering is to suspend a neutrally buoyant scatterer of light which undergoes translatory motion (along with the water) in response to a sound wave. This motion may then be detected with the Doppler effect though there are at least two problems: (i) relative to the proposed bubble mechanism the sound amplitude required to produce the displacement of one fringe may be large and (ii) the light may be subjected to phase disturbances when traveling to and from the scatterer which would produce a background modulation. For the proposed fine-structure bubble mechanism, it is anticipated that the phase disturbances of the intermediate media will be less of a problem. This is because the light which interferes has been reflected from two different sides of the bubble. Phase shifts due to propagation to and from the scatterer should not greatly effect the sensitivity. An order-of-magnitude estimate suggests that there will be a somewhat larger fringe shift with the bubble method than with the neutrally buoyant scatterer method though it is necessary for the sound to be at a frequency below the resonance frequency for the bubbles.

F. Forward Scattering of Light from Bubbles in Liquids

This work was carried out in 1984 as part of the Ph.D. dissertation project of D. S. Langley.[13] During the past year brief descriptions of the experimental results were published.[C1,C3] Langley has been preparing a more detailed description of the experiment and of the theory but has been delayed by a move from Whitman College to the physics faculty of St. John's University (Collegeville, MN).

V. PRODUCTION OF SOUND BY A PRE-EXISTENT BUBBLE IN WATER ILLUMINATED BY MODULATED LIGHT: A NOVEL PHOTO-ACOUSTIC SOURCE AND RELATED EXPERIMENTS ON THE OPTICAL LEVITATION OF BUBBLES AND ON THE SOUNDS PRODUCED BY ILLUMINATED DROPS (B. T. UNGER)

A. Review and Summary

The previous Annual Summary Reports[3,G1] describe experiments and a simple model for the production of sound by bubbles in water illuminated by modulated laser light. These experiments and the development of appropriate theories for the sound radiated from drops and bubbles were the Ph.D. dissertation problem of a graduate student B. T. Unger. Unger completed his dissertation[H1] in December 1986. At the same time he completed the State's requirements to certify as a public school teacher. From January - July 1987, Unger worked part-time towards the completion of manuscripts on this work for publication while supporting himself primarily through temporary or part-time teaching assignments. He has recently moved to the Seattle-Tacoma area where he is seeking employment in education. Only a brief outline of the progress will be noted here since his dissertation[H1] is available from University Microfilms (Ann Arbor, MI) and in the content of forthcoming publications.

B. Sounds Radiated by a Dyed Oil Drop in Water Illuminated by Modulated Laser Light

In the experiments the drops had diameters L typically of about 3 mm and the laser beam was much smaller in diameter. The drops were surrounded by a bath of clear water. The power $P(t)$ of the laser beam (green light) was modulated to produce either a single pulse or a sequence of square pulses each of duration τ separated from each other by a dark interval of duration also of τ. For cases where the sequence is long enough for the sound to build up to the steady state response, $P(t)$ could be taken to be a square-wave of infinite duration which has the following Fourier series representation

$$P(t) = (P_o/2)\left\{ 1 + (4/\pi)\sum_{n=1,3,5...} n^{-1}\sin(n\omega t) \right\} \tag{9}$$

where $P_0 \approx 0.8$ Watt was the peak optical power during the pulse, $\omega = 2\pi f$, and $f = (2\tau)^{-1}$ is the fundamental modulation frequency.

During the past year Unger and Marston developed a semiquantitative thermoacoustic theory for estimating the sound pressure level at a distance $R \gg L$ from the drop. For the $P(t)$ given by Eq. (9) the pressure is given by a series of harmonics

$$p(R,t) \approx (F\beta\, P_o\alpha L f/c_p R\pi)\sum_{n=1,3...}^{N} \cos\left[n\omega(t-R/c)\right], \tag{10}$$

where

β	=	thermal expansion coefficient of the oil
c_p	=	specific heat capacity of the oil
c	=	sound speed in water
α	=	optical absorption coefficient of the dyed oil
$P_o\alpha L$	=	approximation for the optical power absorbed by the drop while the beam is on (this assumes that $\alpha L \ll 1$)

In one version of the model $F = 1$ while a second method of derivation (based on different assumptions) gives $F =$ (density of water)/(density of the oil) ≈ 1.14. The data mentioned below is in better agreement with the theory having $F = 1$. The termination of the series after N harmonics reflects the finite bandwidth used in the experiment. In most cases the bandpass filter was set such that only the $n = 1$ harmonic is recorded.

Figure 11 shows representative recorded output of the hydrophone for the case of a single pulse of illumination (upper figure) and to a sequence of four pulses (lower figure). In each case the fundamental frequency $f = 150$ kHz. The lower figure (together with bandwidth considerations) suggests that four pulses were more than sufficient to bring about a steady state response. The central question becomes "How well does the semi-quantitative theory, Eq. (10), do in predicting the pressure peak-to-peak amplitude?" The comparison yields an average value for the ratio

$$P_{experiment}/P_{theory} \approx 0.23, \tag{11}$$

with $F = 1$ in Eq. (10). This result is an average for 14 drops with this ratio in the range 0.19 to 0.30 for most drops. Systematic sources of error capable of explaining the entire discrepancy have yet to be identified. Consequently it appears that the present model overestimates the radiated amplitude. It is important to note that several assumptions made in the derivation of Eq. (10) are not strictly valid and to develop a more complete theory would not be a trivial task. (The theory neglects drop resonances.) There may be a reduction of the signal due to the method of supporting the drop. Also, some experiments[H1] clearly show that a nonthermoacoustic mechanism can be present for drops.

A manuscript has been prepared which is descriptive of this work but it is not in its final form as of the time of this writing.
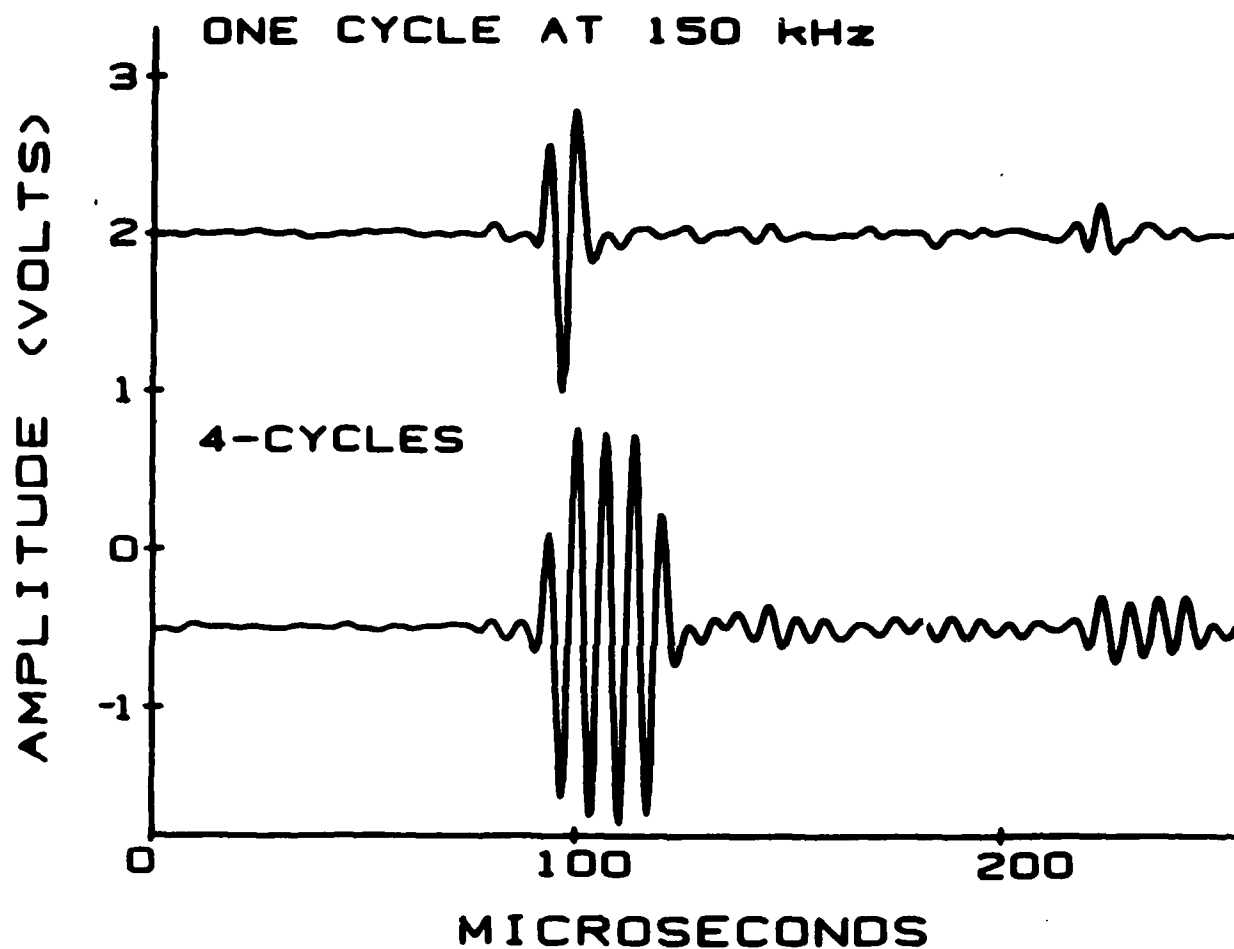
Fig. 11. Records of acoustic signals radiated from a dyed oil drop in water. In the upper curve the drop was illuminated by a single optical pulse while in the lower curve the illumination was a burst of four pulses. The peak optical power was 0.8 W and the drop diameter was 2.99 mm. Each pulse was of duration 0.5 $(150 \text{ kHz})^{-1}$ = 3.3 μsec.

C. Optical Levitation of Bubbles in Water by the Radiation Pressure of a Laser Beam: An Acoustically Quiet Levitator

Early in this effort optical levitation of bubbles was developed as a method for quiet levitation of a bubble in water. Unfortunately, the technique was not used extensively for photoacoustic experiments because of the failure of one of the Ar-Ion lasers. Nevertheless the technique is novel and sufficient data was acquired to support a semiquantitative model of its operation. Hence a manuscript descriptive of this work was completed and submitted for publication.[B3] This includes an improved derivation of the model.

D. Optically Stimulated Sound from Gas Bubbles in Water

This was the central topic of Unger's dissertation.[H1] As noted in Section VC above, the optical radiation pressure on a bubble can be sufficient to prevent a bubble from floating up to the top surface in a tank of water. That same pressure should also squeeze the bubble.[3,G1] The radiation pressure is modulated along with the optical power of the beam and in response to this modulated pressure the bubble is set into radial pulsations. These pulsations in turn radiate sound. Representative records of the sound were shown in a previous Annual Summary Report.[3] Unlike the case of drops (Sec. VB) the radiation from bubbles is dominated by the properties of the monopole resonance.[3] For steady-state measurements described below the modulation is a square wave described by Eq. (9) with a fundamental frequency f. It has been shown that the steady-state pressure is maximized when f corresponds to the frequency of the bubble's monopole resonance.

The principal new research carried out during the present contract period was as follows[H1]: (i) an improved calculation of the radial projection of the radiation pressure for the optical beam profile used; (ii) a check of certain aspects of the calibration procedure so as to reduce systematic errors in the amplitudes measured in the experiment; (iii) comparison of experimental and predicted acoustic pressure amplitudes for a wider range of

parameters; and (iv) development of a novel way of plotting the amplitude data to test the coupling mechanism.

For the purpose of the present discussion, attention will be restricted to items (iii) and (iv) with initial discussion being of item (iv). In the experiments, the irradiance profile for a beam was minimized on the beam axis (a "doughnut" mode beam). This had the effect of putting most of the beam power in the total reflection region of the bubble's surface. The goal of the experiments to be described is to show how the acoustic pressure radiated depends on a/w where a is the bubble radius and w is a parameter which describes the effective radius of the beam. It is assumed in the calculation that w is fixed while a is varied. For each value of a the modulation frequency f is adjusted to correspond to the bubble's radius. The resulting estimate of the radiated pressure (normalized to that of the maximum amplitude) is shown as the curve in Fig. 12. It turns out that for a wide range of widths w, the predictions fall on the same curve (shown) which is a function primarily of a/w. The reason for the reduction in pressure for large values of a/w is that the bulk of the beam power is transmitted through the center of the bubble and the intensity is low in the total reflection region (which lies near the region where the local impact parameter of a ray is large). Consider now the data (the points) where the various methods of supporting the bubble are indicated. The data have the general shape of theory. What is most important is that observed ratio p/p_{max} falls off when a/w is large. This would not be the case if the mechanism were a thermoacoustic mechanism which involved the periodic heating of gas within the bubble. When a/w is large there is more light transmitted to the gas within the bubble. (The method of collecting the data did not allow for direct measurement of w but w was inferred through the value of a/w which maximized the acoustic signal. (See Ref. H1.)

Though Fig. 12 strongly supports that radiation pressure is the mechanism whereby the radial pulsations of the bubble are driven, a significant puzzle remains. The measured
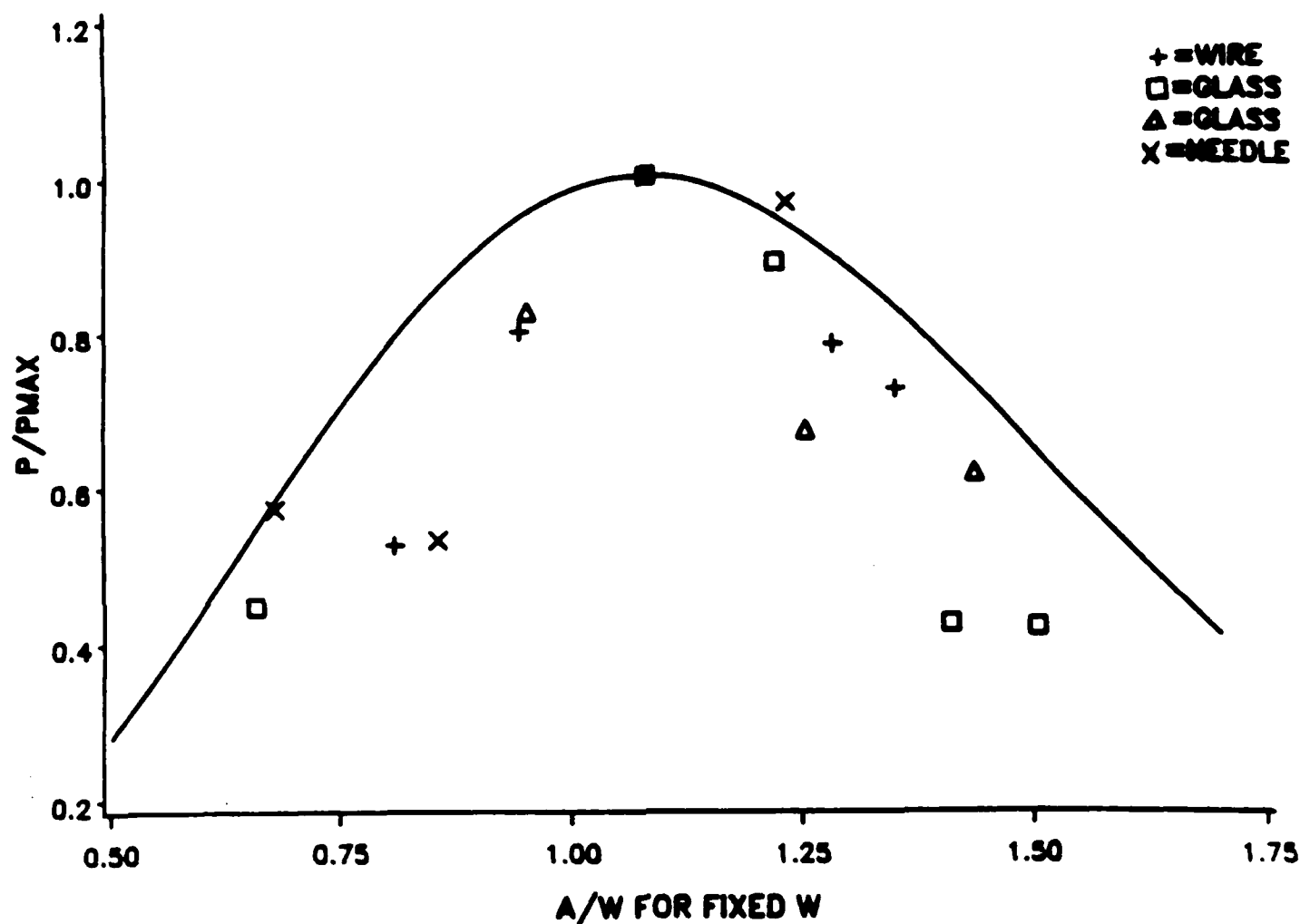
Fig. 12. Normalized acoustic pressure amplitude radiated by an illuminated bubble as a function of the bubble radius-to-beam width ratio a/w for data sets each corresponding to a fixed beam width w. The solid curve is from the optical radiation model for the excitation of bubble oscillations. The vertical scale is adjusted so that all data sets correspond to the model at the maximum (the black square). This plot appears to support modulated optical radiation pressure as the mechanism for driving the bubble oscillations and the resulting radiation of sound. The method of supporting the bubble is indicated by the symbol type.

magnitude of the radiated sound wave typically exceeds the predicted magnitude by a factor of 10. The prediction uses the same radiation pressure theory that gives the curve in Fig. 12. At present, the reason for this discrepancy is not known. It appears not to be a simple matter of hydrophone calibration since the same calibration gave the results in Eq. (11) for the pressure-radiated from drops.

VI. ACOUSTICAL AND OPTICAL DIFFRACTION CATASTROPHES

A. Motivation and Review

Diffraction catastrophes are a class of foci or caustics which occur in various acoustical and optical problems.[1-3,G1] They are important for describing the wavefield since purely geometrical propagation rules give unphysically divergent amplitudes at caustics in the short wavelength limit. As noted below, the resolution of issues raised during these optical scattering experiments has advanced the understanding of acoustical diffraction catastrophes.[A1,A2,G1] The emphasis of the present research is on specific caustic manifestations including the ways in which acoustic echoes merge at caustics. In reflection experiments the merging of echoes provides a simple way of locating caustics.

In addition to contributions to specific areas mentioned below, it is noteworthy that graduate students C. Dean and P. Arnott have assisted with the computer graphics used throughout the work on catastrophes.

B. Surface Shapes Giving Transverse Cusp Catastrophes in Acoustic or Seismic Echoes, the Caustic Surface, and Optical Simulations

In the previous research[3,A1,G1] the generic shape of wavefront was identified which propagates to produce a transverse cusp caustic.[14] During the present contract period that analysis was extended so as to obtain the caustic parameters for transverse cusps produced by the reflection of sound from smooth curved surfaces. The sound is assumed to be initially radiated from a point source. A manuscript on this problem[D1] is

Fig. 13. The upper photograph shows one perspective of the optical reflection experiment used to simulate acoustical transverse cusps. A beam diverges from the lens on the right so as to reflect from the smooth curved surface on the left. The resulting transverse cusp caustic is visible on the ground glass screen near the center of this photograph. In the lower of the photographs the camera is positioned so as to view the glints from the reflecting surface. This positioning of the camera is similar to that of Fig. 6 of Appendix I except that here the aperture lies close to the caustic surface and two of the glints have merged.

included as Appendix I of the present report and the reader is referred to Figs. 2-5 of that appendix for illustrations of the geometry. The parameters of the caustic surface for the reflected rays are implicit in Eq. (20) of that appendix.

In addition to that analysis, Appendix I also describes a simple optical simulation of transverse cusps produced by reflection. (This simulation was carried out with the assistance of graduate students C. Frederickson and W. P. Arnott.) Figure 13 of the present report shows two photographs of the simulation. The upper photograph is an overview of the apparatus. The laser and lens (visible on the right) produce a diverging beam which simulates the point source. The screen displays the transverse cusp. The simulation demonstrates that the transverse cusp and caustic surface have qualitative features like those predicted. [For a detailed description, see Fig. 6 of Appendix I and the sections titled "OPTICAL SIMULATION OF ACOUSTICAL TRANSVERSE CUSPS" and "LOCATING CAUSTICS BY THE MERGING OF RAYS . . .".] The lower photograph of Fig. 13 shows how two rays to the camera's aperture (these correspond to "glints" in the photograph) merge after that aperture has been moved upward to lie on the cusp curve. (Compare with Fig. 6 of Appendix I and the section on "LOCATING CAUSTICS . . .".) The merging glints are visible in the upper part (of the lower photograph) of Fig. 13.

C. Hyperbolic Umbilic Focal Sections: The Wavefields and the Merging of Rays at Caustic Lines

In Sec. IVD of the previous Annual Summary Report,[G1] a new method for obtaining wavefront parameters in scattering problems was described which was based on Kneisly's method[15] for tracing the local principal curvatures of wavefronts through an optical system. This method was then applied to new results (Sec. IVC of that report) relating the wavefront parameters to the caustic parameters for the hyperbolic umbilic focal

section (h.u.f.s.). When applied to the specific case of the h.u.f.s. diffraction pattern seen in light scattered from oblate water drops,[9,16] the result for the apex angle between the caustic lines was in good agreement with the observations.[F3] The calculation was not trivial because there are two (oblate) refracting surfaces and one (oblate) reflecting surface.

During the present contract period the calculation was carried to the next level of sophistication: the wavefield in the h.u.f.s. was calculated and compared to photographic records[9,16] of the diffraction pattern. The result shows good agreement between theory and experiment without the use of any adjustable scaling parameters in the model (though in the experiment the absolute scattering angle could not be measured though the increment in scattering angle was measured).

The method of calculation is outlined as follows. The notation used is that for acoustical diffraction catastrophes.[A1] Recall that Marston demonstrated that the general shape function $g(x,y)$ for the outgoing wavefront is of the form[G1,D2,F3,F7]

$$g(x,y) = \left[(\alpha x^3 + 3\gamma y^2 x)/6\right] + a_1(x^2 + y^2), \tag{12}$$

where the parameters are such that α and γ are of the same sign and $a_1 \le 0$ since the distance from the xy plane to the focal section is $z_{fs} = -(2a_1)^{-1}$. The basic geometry is illustrated in Fig. 14. The angle ψ between the caustic lines is[G1] $\psi = 2 \arctan\beta$ where $\beta = (\gamma/\alpha)^{1/2}$. The pressure in the exit plane is the real part of[A1]

$$p(x,_\jmath,t) = e^{ikg(x,y)}e^{-i\omega t}, \tag{13}$$

where $k = \omega/c$ and the wave is of unit amplitude. The formulation of the diffraction problem is like the one described in Ref. A1 and Appendix I for the transverse cusp except that the dimensionless diffraction integral F becomes

$$F = \int\int_{-\infty}^{\infty} \exp\left\{ik\left[\frac{1}{6}(\alpha x^3 + 3\gamma y^2 x) - (xu + yv)z^{-1}\right]\right\}dxdy \tag{14}$$
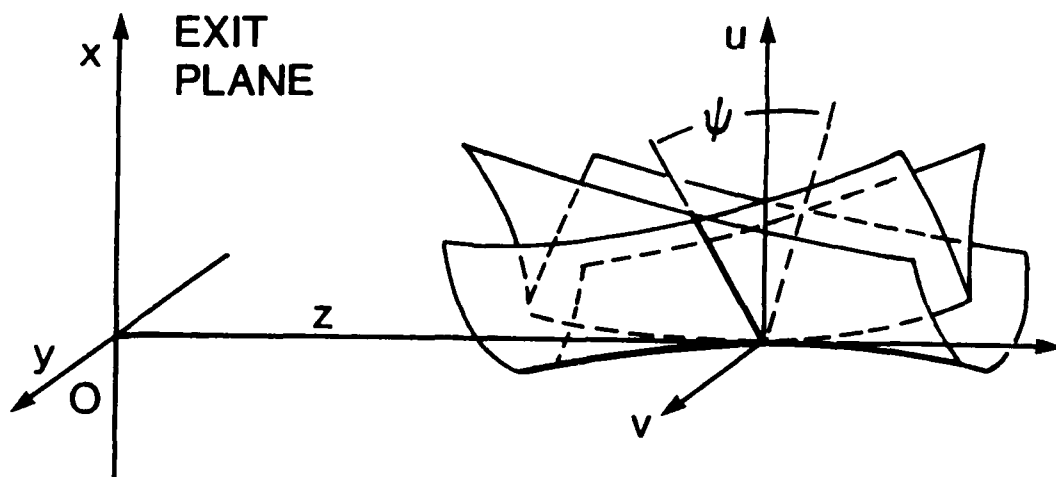
Fig. 14. Caustic surface for a hyperbolic umbilic diffraction catastrophe for the case where the distance z_{fs} to the focal section (the uv plane) from the exact plane (the xy plane) is finite. The shape function of the outgoing wavefront at the exit plane is given by Eq. (12) with $a_1 < 0$ for the case shown.

where here and below it is assumed that the observation plane is the focal section ($z = z_{fs}$).

The diffracted pressure is the real part of[A1]

$$p(u,v,t) = \frac{k}{2\pi i r} F e^{ikr} e^{-i\omega t}. \tag{15}$$

Marston has evaluated (14) by carrying out a shearing of coordinates with the result[F7]

$$p = \frac{k^{1/3} 2^{4/3} \pi}{i r \alpha^{2/3} \beta} e^{ikr} e^{-i\omega t} Ai(q_1) Ai(q_2). \tag{16}$$

$$Ai(q_j) = \frac{1}{\pi} \int_0^\infty \cos(\frac{1}{3} s^3 + q_j s) ds, \tag{17}$$

$$q_j = - \frac{k^{2/3}}{(2\alpha)^{1/3}} \left(\frac{u}{z} \pm \frac{v}{z} \beta^{-1} \right), \quad j = 1,2, \tag{18}$$

where $Ai(q_j)$ is the standard Airy function for the real argument q_j.

All of the above can be applied to the light scattering problem of an oblate drop where p describes the dominant component of the electric field. To carry out this application it was necessary to use certain of the previous results for the shape parameters of the outgoing wavefront[G1]

$$\beta = \frac{m}{\sqrt{12}}, \quad \alpha = \frac{18}{D^2} \frac{(4-m^2)^{1/2}}{(m^2-1)^{3/2}} \tag{19}$$

where D is the diameter of the drop in the equitorial plane and $m = 1.332$ is the refractive index of the drop. Figure 15 superposes on the observed pattern a contour plot of a function proportional to $Ai(q_1) Ai(q_2)$, and hence to the field. The actual irradiance is proportional to $|Ai(q_1) Ai(q_2)|^2$. The calculations and observations are for the far-field ($z \to \infty$) limit. The agreement is remarkable considering the nature of the experiment.

Fig. 15. (on next page) Comparison of experiment and theory for the hyperbolic umbilic focal section scattering pattern for light scattered from an oblate drop of water near the angle of the rainbow. The photograph in the background is from the experiments described in Refs. 9 and 16. The contour plot is of the function $S = Ai(q_1) \, Ai(q_2)$ where q_1 and q_2 are given by Eq. (18) and Ai is the Airy function. The solid contours are for regions where $S > 0$ while the dashed contours are for regions where $S < 0$. The irradiance should be proportional to S^2. The agreement between theory and experiment for regions of high irradiance is noteworthy considering the experimental difficulties in determining an accurate drop diameter D and because of the complexity of the theory. The light is refracted or reflected by three curved surfaces before leaving the drop. This complicates the calculation of the apex angle ψ and made it necessary to use the method of wavefront tracing introduced in the previous Annual Summary Report.
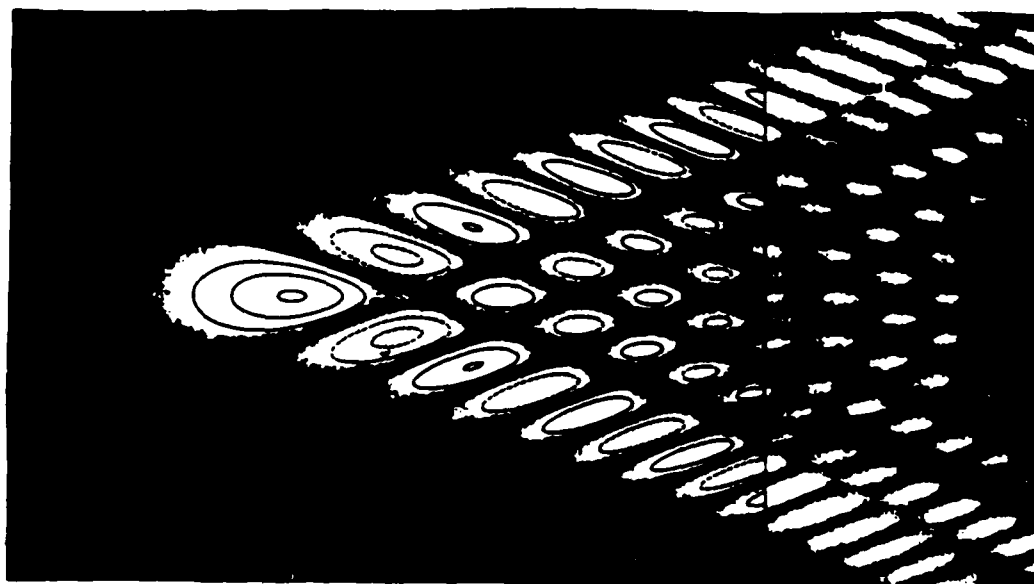
5 deg

One of the difficulties in understanding the h.u.f.s. is to explain the way in which the rays merge as the observation point (u,v) in Fig. 14 crosses the caustic lines in the focal section (at fixed $z = z_{fs}$). As (u,v) crosses these lines the number of rays must drop from[16] 4 to 0. It is reasonable to ask "How do these rays merge and disappear?" This problem was solved by applying a method previously introduced by Marston in Sec. III of Ref. A1 for the case of transverse cusps.[F7]

D.   Applications to the Theory of Shock Wave Focusing

Some applications of catastrophe theory to the theory of focused shock waves were considered.[D2] The starting point was to apply catastrophe theory concepts to describe the caustic surfaces for intrinsically three-dimensional linear waves. (The two-dimensional problem of a weakly-focused converging cylindrical wave was reviewed in Ref. D2 and in Fig. 1 of Appendix I.) In this case the caustic is a longitudinal cusp (an arête). The analysis for the linear problem faci''tated the connection of the shape parameters for the outgoing wavefront with the classification of the caustic surface and the description of the parameters which characterize the caustic surface.

The connection between these linear propagation problems and the focusing of real shock waves (in gases or in liquids) may be seen as follows. It is appropriate to first make note of experiments[17] and recent computations[18] of the focal properties of cylindrical nonlinear shock for a cylindrical bulge as illustrated in Fig. 1 of Appendix I for the linear case. Nonlinear effects tend to defocus rays which would otherwise form the arête. As the concave forward portion of the wave strengthens, it speeds up so as to reduce the bulge. Hence rays are not straight as assumed for acoustic shocks. Experiments[17] and computations[18] show, however, that real cylindrical shocks can become unstable with respect to the formation of a pair of shock-shocks in the focal region; a Mach-stem-like section connects these shock-shocks. Evidently, the rate at which a bulge is reduced is not

always rapid enough to prevent Mach intersection of the obliquely convergent shocks in the focal region. The important point here is that nonlinear effects become important in the focal region and the way they are manifested is not trivial to predict.

The simplest of the three-dimensional linear focusing problems considered was the transverse cusp caustic surface as illustrated in Fig. 5 of Appendix I. If, instead of linear shock wave propagation, the wave is taken to be a nonlinear shock wave having the same initial shape, it is clear that the effects of the nonlinearities must become important in the focal region. The way these will be manifested is not presently clear. For example, the converging wave could become unstable with respect to the formation of shock-shocks.

E. Calculation of the Principal Curvatures of Wavefronts and Their Applications to Transverse Cusp Diffraction Catastrophes (C. Dean and W. P. Arnott)

In the usual formulation of catastrophe optics[10,19] the principal curvatures κ_1 and κ_2 of a wavefront and the associated Gaussian curvature $\kappa_g = \kappa_1\kappa_2$ are approximated with the aid of a paraxial assumption where the local slope of the wavefront is taken to be small. On the other hand, Kneisly's method[15] of tracing the wavefront does not require the use of a paraxial assumption. It appeared desirable to obtain general expressions for κ_1, κ_2, and κ_g from equations for the wavefront (or other surface shape) in cartesian or polar coordinates for points on the surface. Oddly enough the required general expressions could not be found even after consulting several texts and reference books on classical differential geometry. Consequently C. Dean and W. P. Arnott obtained novel general expressions for κ_1, κ_2, and κ_g which do not make use of a paraxial assumption. These expressions were tested against several standard cases and found to give exact results. A manuscript descriptive of this calculation is in preparation.

Recall from Sec. VIC and from the previous Annual Summary Report[G1] that the shape parameters for the case of the hyperbolic umbilic wavefront were found and related to the caustic parameters. (For the hyperbolic umbilic the shape parameters are the α and γ of Eq. (12).) C. Dean has been working on a similar calculation which would enable the calculation of the shape parameters from the principal curvatures κ_1 and κ_2 for those wavefronts[A1,D1,D2] which give transverse cusp caustics. Here the eventual goal is to find the opening rate for the caustic from surface properties of the reflecting or refracting system. A special case of this problem was solved by Marston for the reflection geometry shown in Fig. 4 of Appendix I. (There the opening rate is proportional to the multiplicative factor on the left side of Eq. (20) of Appendix I.) A specific (and more difficult) problem considered by C. Dean is the calculation of the opening rate for the transverse cusp caustics observed in the scattering from spheroidal drops of water.[9] This calculation is to be checked against existing data.

Once the caustic parameters and wavelength is known for a transverse cusp diffraction catastrophe, the wavefield may be expressed using the Pearcey function

$$P(X,Y) = \int_{-\infty}^{\infty} \exp\left[i(s^4 + s^2 X + sY)\right]ds. \tag{20}$$

Computer algorithms to evaluate this function are not widely available. One of C. Dean's current tasks is to adapt an algorithm kindly supplied to us by Professor F. J. Wright[20] (University of London) to allow $P(X,Y)$ to be computed here at W.S.U. This is needed to compute the diffraction pattern in the light scattering experiments and the steady-state wavefield in the acoustic reflection experiments described in the next section.

F. Experiments with Acoustical Transverse Cusps Produced by Reflection from Smooth Surfaces (C. K. Frederickson)

During the period May 15, 1987 - August 15, 1987 a graduate student, C. Frederickson, began experiments on acoustical transverse cusps[A1] produced by reflection. Frederickson is to resume experiments in January 1988 as he works toward the completion of a M.S. degree in physics; hence only a brief summary of the present results will be given here. The goal is to demonstrate experimentally various properties of steady-state and transient wavefields near transverse cusp caustics, some of which are predicted in Ref. A1 as well as Appendix I and Sec. VIB of the present report.

The first task was to set up a new water tank facility with sides spaced farther apart than for the existing 300 gallon tank. This tank was needed to reduce the problem of spurious wall echoes both for the catastrophe experiments and the phase conjugation experiments discussed in Sec. VII. Figure 16 shows the new tank which was made by cutting the top off of a 550 gallon cylindrical polyethylene tank manufactured for the storage of agricultural liquids.[21] After removal of the top the capacity is 500 gallons, with a diameter and typical liquid depth of 168 cm and 83 cm, respectively.

Figure 16 also shows a smooth curved acoustic reflector immersed in the tank. The reflecting surface is a thin air-backed polished metal sheet supported by a sealed lucite frame. The design is similar to that of the optical reflector shown in Fig. 13 and Appendix I, Fig. 6. For this reflector the surface height function, Eq. (15) of Appendix I, reduces approximately to the following form

$$h(x,y) \approx c_2 y^2 x, \qquad c_2 \approx -0.0008 \text{ cm}^{-2}, \tag{21}$$

In the section on "TRANSVERSE CUSPS PRODUCED BY THE REFLECTION FROM SMOOTH CURVED SURFACES," it is shown that sound radiated from a point source which reflects from such a surface, should produce a transverse cusp caustic described by
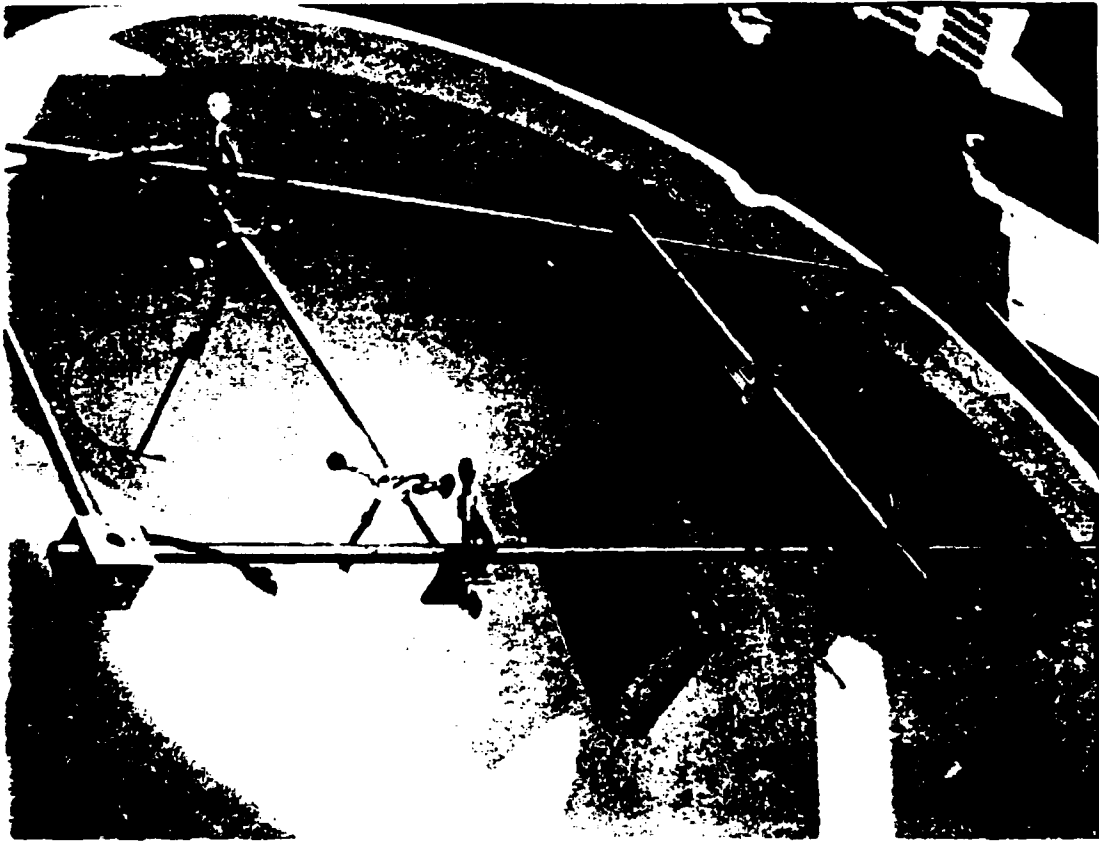
Fig. 16. Photograph of the new tank facility. The rail supports shown have the same spacing as for the old facility so that various hydrophone mounts or target holders may be transferred back and forth between tanks.

Eq. (20) of Appendix I. Though the form of the wavefield is calculated there for the case of a steady-state sine wave, the present experiments were concerned only with merging of transient echoes as discussed in the section "LOCATING CAUSTICS BY THE MERGING OF RAYS AND OF PULSED ACOUSTIC ECHOES," in Appendix I. Since that section outlines the theory, the discussion below will summarize only the present status of the experiments.

The geometry of the experiment is as shown in Fig. 4 of Appendix I where the source is located at an effective distance $z_s \approx 105$ cm from the reflector such that the transverse coordinates are $u_s = 0$, $v_s = 0$. The diverging wave is radiated from a curved piezoelectric transducer driven by a single cycle of a 2.5 MHz sine wave. The receiver hydrophone was scanned in a plane at a distance $z = 80$ cm from the reflector. For the time records to be discussed, Fig. 17 illustrates the receiver locations relative to the inferred position of the cusp caustic. The hydrophone was scanned vertically along the line shown and the records of the hydrophone output are as shown in Fig. 18. Each record was triggered at the same time relative to the emission of the sound from the source. Records (a) and (e) were taken deep in the one-ray region of the reflection. In each case only a single echo, labeled (1), is clearly displayed. Record (c) is for the hydrophone located within the cusp in the three-ray region. Since the position is shifted from the symmetry axis of the cusp, none of the echoes should have the same arrival time and this is evidenced by the broad signal labeled (1) + (2) + (3). Unfortunately the time resolution is insufficient to resolve three distinct echoes. The late echo in (c) is evidently due to scattering from an edge of the reflector. In record (d) the hydrophone has been lowered to lie close to (or on) the cusp curve. Two of the echoes have merged to produce the large echo labeled (2 + 3) which clearly arrives earlier and distinct from the smaller echo labeled (1). A similar merging is shown in record (b) which is for the hydrophone located on or near the upper cusp curve.

Fig. 17. (on next page) Position of the hydrophone relative to the apparent cusp curve position for the records shown in Fig. 18. The position labeled (A) gives the record in Fig. 18(a), (B) gives the record in Fig. 18(b), etc. The hydrophone outputs recorded in Fig. 18 are shown having a fixed voltage amplification factor.

(A) •

(B) •

(C) •

(D) •

5 cm

(E) •
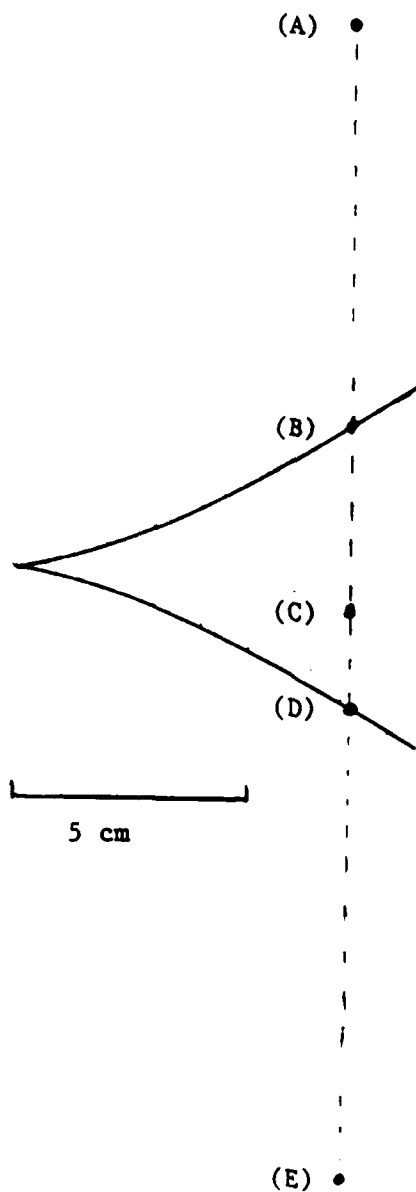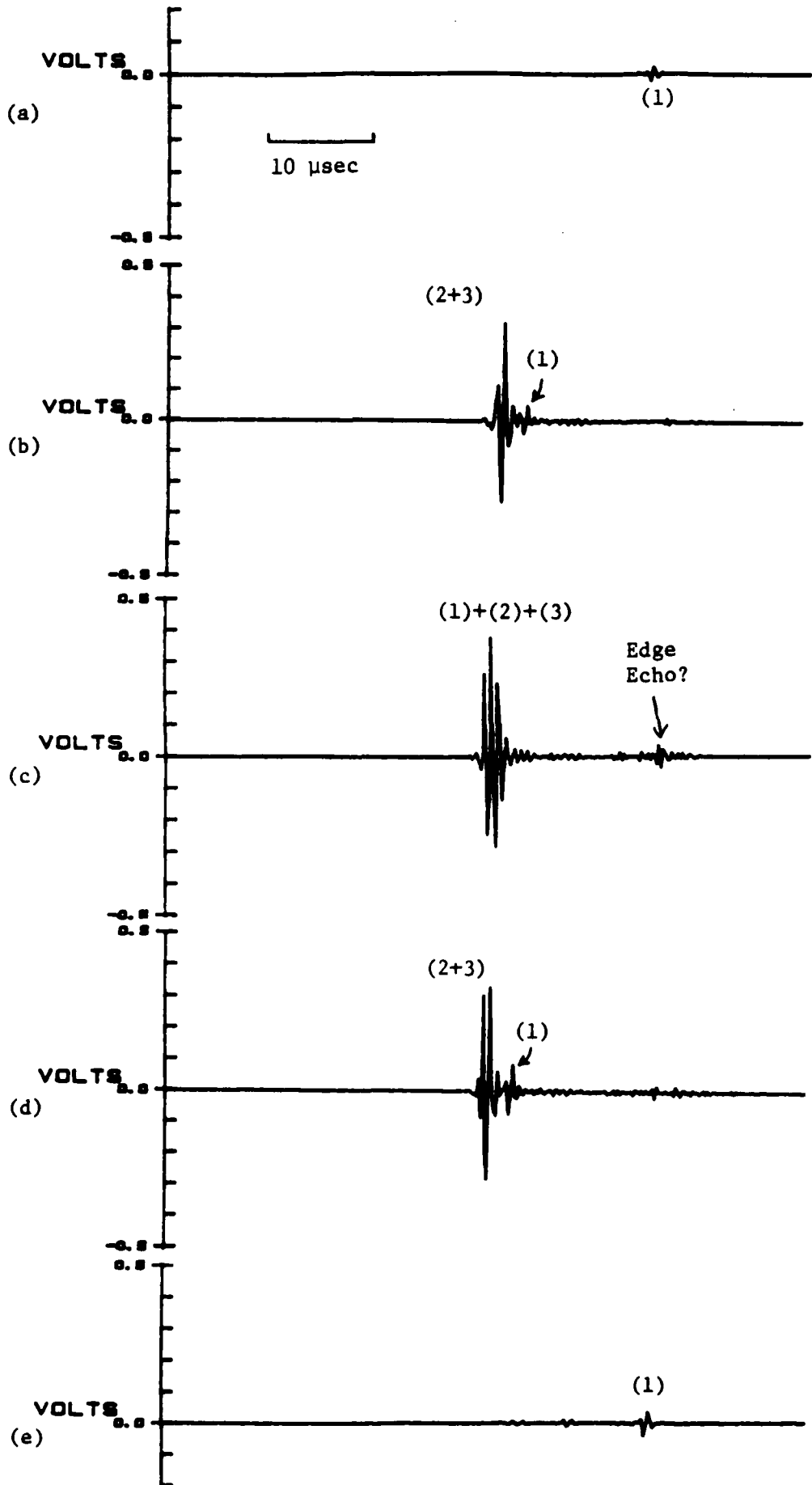
Fig. 18. See caption to Fig. 17.

Continuous transitions were observed in the records as the hydrophone was moved along the paths (b) to (a) and (d) to (e). In each case the echo labeled (1) was continuously visible but had a gradual reduction in amplitude. The arrival time increased monotonically with the apparent distance from the symmetry axis from the cusp as is to be expected from the theory. The echo labeled (2 + 3) remained distinct from echo (1) and undergoes a much larger reduction in its amplitude such that it can be no longer seen for hydrophone positions (a) and (e). This behavior is also consistent with the theory as the receiver is shifted to lie deep within the one-ray region.

Additional features observed are in qualitative agreement with the theory. For the distance parameters z_s and z of this experiment and the estimated value of c_2 in Eq. (21), application of Eq. (20) of Appendix I predicts that the cusp point should lie about 7 cm to the left of the scanned line shown in Fig. 17. The hydrophone was moved at (or close to) the predicted cusp point location and in agreement with expectations the dominant feature of the output was a large-single-echo. In addition, application of Eq. (23) of Appendix I gives the following prediction for the relative arrival times when the receiver is located at positions (b) and (d) which are assumed to lie on the cusp curve. The prediction is that echo (1) should be delayed relative to echo (2 + 3) by 3.7 μs. The apparent observed delay was 2.3 μs which suggests that either this preliminary demonstration of locating the caustic contained errors (in the inferred position of the caustic) or that the parameter c_2 was not known to sufficient accuracy.

It should be noted that experiments had been previously carried out by Hilterman[22] which illustrated the merging of reflection echoes at a longitudinal cusp caustic. Those experiments were carried out for propagation in air for sound produced by a spark source. Figure 1 of Appendix I, shows the geometry of merging rays for the longitudinal cusp. This is essentially different (and simpler than) the case of a transverse cusp since the rays for the longitudinal cusp are confined to lie in a plane.

To facilitate the experiment described in Fig. 17 and 18, Frederickson modified an analog x-y recorder so that it could be used to give a two-dimensional scan of the hydrophone.

Frederickson carried out experiments intended to be useful for the imaging of the steady-state wavefield near the cusp. The basic idea is that a sheet of paper is immersed in dyed water and subjected to a high frequency sound field. The dye (methylene blue) is most rapidly absorbed by the paper in regions where the sound field is the most intense.[23] Hence, if the paper is removed from water, it should be left with a dye pattern which "images" the sound field. By placing a sheet in front of a transducer designed to give a line focus, Frederickson observed that a blurred line image appeared on the paper. Unfortunately the tests seem to indicate the contrast in the image is not sufficient for the present application of imaging diffraction catastrophes; however, a broad range of parameters were not explored.

VII. ACOUSTICAL PHASE CONJUGATION

A. Review and Theory Development

In Sec. VII of the previous Annual Summary Report,[G1] various mechanisms for producing acoustical phase conjugating mirrors (PCM) are discussed. A PCM is a mirror which reverses the outgoing wavefront so that it propagates back toward the source. The experiments under way here at the time of this writing make use of a form of bubble layer (see the next subsection) for the nonlinear medium where the interaction occurs. Hence the present theoretical discussion will consider only recent developments related to that mechanism.

Before discussing the present status of the experiments it is appropriate to review the problem of the focal-point shift for the reversed wave introduced by Marston in the previous Annual Summary Report. The geometry to be considered here is illustrated in

Fig. 19. A thin layer of bubbles is confined to a plane at $z = 0$ and it is in this plane where the nonlinear interaction of pump (1), probe (2), and reversed wave (3) takes place. The pump and probe waves are taken to diverge from points at distances z_1 and z_2 from the bubble layer. The following analysis was motivated by the publication of Soviet experiments,[24] claiming to detect a reversed wave, but making no mention of the problem of the focal point shift. If f_1 and f_2 denote the frequencies of the pump and probe waves, the frequency of the reversed wave for the class of nonlinear interaction considered (three-wave mixing) is

$$f_3 = f_1 - f_2. \tag{22}$$

In the published experiments,[24] $f_1 = 100$ kHz, $f_2 = 60$ kHz, and $f_3 = 40$ kHz where evidently the choice of $f_3 \neq f_2$ was made so as to discriminate experimentally between the probe and reversed wave signals.

The basic problem is to calculate the distance z_3 from the bubble layer to which the reversed wave appears to converge. For simplicity we shall restrict our analysis to the case where the pump and probe waves diverge from points which lie on the z axis which is perpendicular to the layer. Figure 19 shows rays from these sources to a given point on the layer which is displaced a distance x from the z axis. Associated with these sources and the ray to the focal point (3) are wave vectors $\vec{k}_j$, $j = 1, 2$, and 3, which have the following magnitudes $k_j = 2\pi f_j/c$ where c is the sound speed in the surrounding media (water). Any shift of the sound speed due to the presence of bubbles is neglected. If there is to be an efficient interaction of the pump, probe, and reversed waves in the layer, the following condition must be imposed on the $\vec{k}_j$, irrespective of the local value of x

$$\hat{x} \cdot (-\vec{k}_3) = \hat{x} \cdot (\vec{k}_1 - \vec{k}_2), \tag{23}$$

where $\hat{x}$ is a unit vector. This becomes
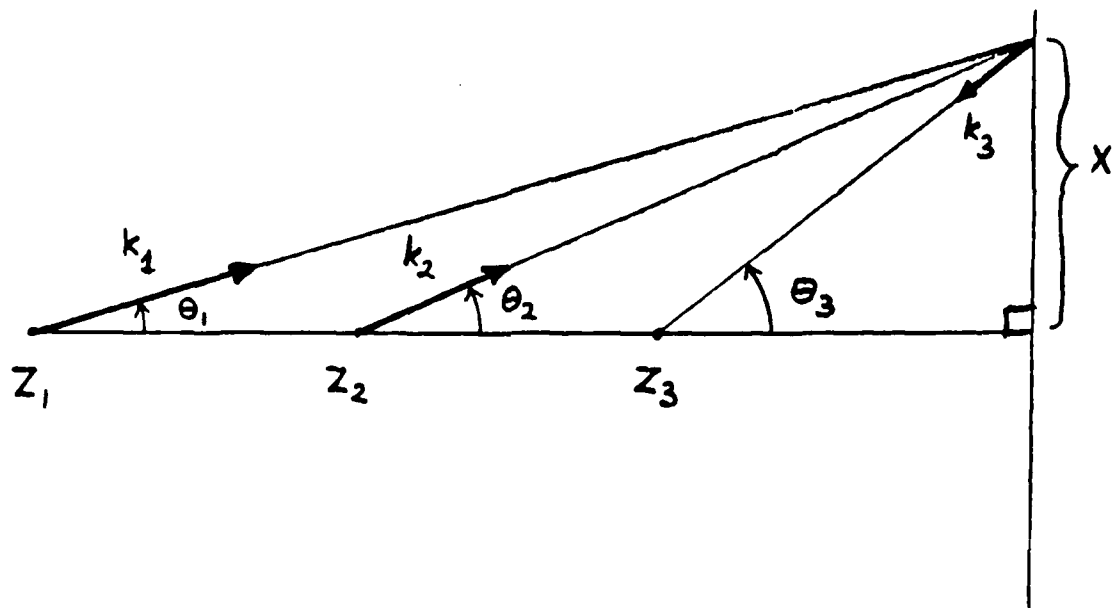
Fig. 19. Geometry considered for a reversed wave (3) which results from the nonlinear
interaction of pump (1) and probe (2) waves at a layer by bubbles in the plane $z = 0$.

$$-k_3 \sin\theta_3 = k_1 \sin\theta_1 - k_2 \sin\theta_2, \tag{24}$$

where the θ_j are the angles relative to the z axis as shown in Fig. 19. In the analysis which follows it is convenient to make a paraxial approximation which assumes that the θ_j are sufficiently small that $(x/z_j) = \tan\theta_j \approx \sin\theta_j$. Then the quantity x may be canceled from both sides of Eq. (24) so that the focal distance z_3 becomes

$$z_3 \approx f_3/\left[(f_2/z_2) - (f_1/z_1)\right], \tag{25}$$

which does not depend on the local transverse location x of the interaction region. For the special case of a plane wave pump beam, $z_1 \to \infty$, so that Eq. (25) becomes[25,G1]

$$z_3 \approx (f_3/f_2)z_2. \tag{26}$$

When $z_3 \neq z_2$, it is appropriate to say that the focal point has been shifted from the source location of the probe wave. Notice that from Eq. (25), even when the reversed wave is taken to have the same frequency as the probe ($f_3 = f_2 = f_1/2$), that $z_3 \approx z_2/[1 - (2z_2/z_1)] \neq z_2$ unless $z_1/z_2 \to \infty$. This "focal point shift" is the simplest form of aberration present for the acoustical phase conjugation mechanism considered.

It is noteworthy that a more recent description and analysis of the Soviet experiments just appeared.[26] This mentions what Marston calls a "focal point shift" and gives an equation which is equivalent to Eq. (25) in the paraxial assumption. The presentation of the data is not sufficiently clear as to say whether a shift was present in what appears to be a reversed wave.

B. Experimental Study of a Reversed Wave (Kargl)

Following the completion in July 1987 of his M.S. degree project[H2] on acoustical scattering (see Sec. IIIC), Kargl began an experimental study of the reversed wave. The discussion of the present results will be brief since they are necessarily preliminary. This presentation is merited because of the observation of a difference-frequency wave.

Furthermore, the discussion is indicative of the present experimental capabilities and the directions to be taken in future research. It should be noted that other mechanisms for generating a reversed wave[1,G1] are to be examined with this apparatus. The experiments are carried out in the new 500 gallon tank shown in Fig. 16 set up by Kargl and Frederickson.

The bubble layer in these experiments consisted of a sheet of Nuclepore[27] filter. This sheet consists of a polycarbonate membrane with uniformly distributed pores running through the membrane. The pore size is sharply defined by the manufacturing process to have a diameter of 10 μm. The manufacturer was to have treated the membrane to make it hydrophobic so the pores will contain a stable gas-filled cavity or microbubble when the sheet is placed in water. Miller[28] demonstrated that similar sheets exhibit a significant nonlinear response to ultrasound though it appears that the generation of sound at the difference frequency was not previously studied. Because the number density of pores may be quite large (according to the manufacturer 10^5 pores/cm^2) it would seem that the associated trapped microbubbles should exhibit the nonlinear response required to mix the signal wave (frequency f_2) with the pump wave (frequency f_1) so as to produce the conjugate wave at frequency $f_3 = f_1 - f_2$. One of the major advantages of this sheet is that it should give a steady population of microbubbles which are sufficiently small that high frequencies ($f_j \sim 1$ MHz) can be used. It is important that the population not fluctuate greatly with time so that background subtraction procedures noted below could be used. The dimensions of the sheet were 20.3 cm x 25.4 cm and the filter was supported at its edges by a thin plastic frame.

Figure 20 is a diagram of the main features of the experiment. The acoustical components (source transducers S_1 and S_2, needle hydrophone R_3, and Nuclepore filter) are not drawn to scale. Power amplifiers A_1 and A_2 amplify sine wave bursts of frequency f_1 and f_2 so as to drive S_1 and S_2. The diameter of S_1 is relatively large

65
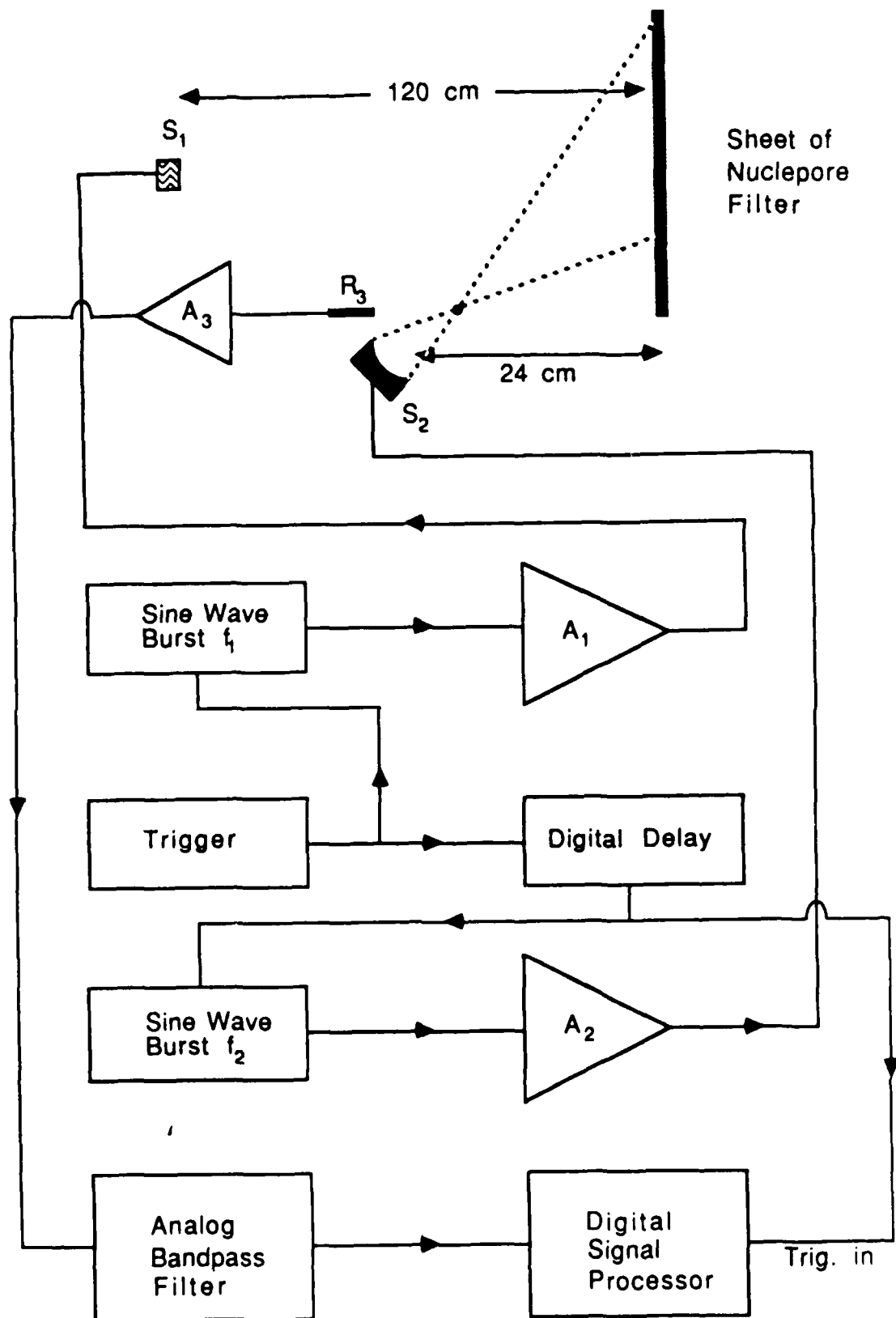
Fig. 20. Phase conjugation apparatus.

(1.5 inches); however, the Nuclepore sheet is in the far field of S_1 so that the pump wave appears to spread from a distance $z_1 < 120$ cm. The burst radiated by the probe source S_2 is delayed so that the pump and probe bursts overlap in time at the center of the sheet as well as on most of the peripheral region pump beam at the sheet. The bursts must be sufficiently short that the hydrophone R_3 and preamplifier A_3 have fully recovered from the outgoing bursts. They should be sufficiently long for the f_1 and f_2 bursts to interact at the filter over different regions in such a way that: (i) the microbubbles in the filter have time to build up to a steady-state nonlinear response; and (ii) the resulting difference frequency waves radiated from different regions of the filter can arrive at R_3 at the same time.

The output of the preamplifier can also be monitored with an analog oscilloscope (not shown in Fig. 20). Direct inspection of this signal during the time window anticipated for the reversed wave shows that appreciable signals are backscattered to R_3 at frequencies f_1 and f_2. Fortunately these signals do not appear to be so large as to drive A_3 into a region of nonlinear response and intermodulation distortion. It is necessary, however, to reduce the amplitudes of these (linear scattering) signals so as to avoid overdriving the digitizer on the digital signal processor so as to be able to pick out the difference frequency f_3 signal which is lower in amplitude. The analog bandpass filter is set to pass the region from f_A to f_B and to attenuate signals with frequencies $< f_A$ and $> f_B$. This filter achieves the required reduction in amplitude by setting $f_3 < f_B < f_2 < f_1$ and $f_A \ll f_3$.

Figure 21 shows signals recorded by the digital signal processor (DSP) for the conditions noted below. The duration of each record is 28.2 μs. The time window recorded was the same for each trace. The trigger delay in the DSP was adjusted so that the time window recorded would include signals radiated from the interaction region of the Nuclepore sheet. The pump wave was a sine wave burst of frequency $f_1 = 2.0$ MHz and
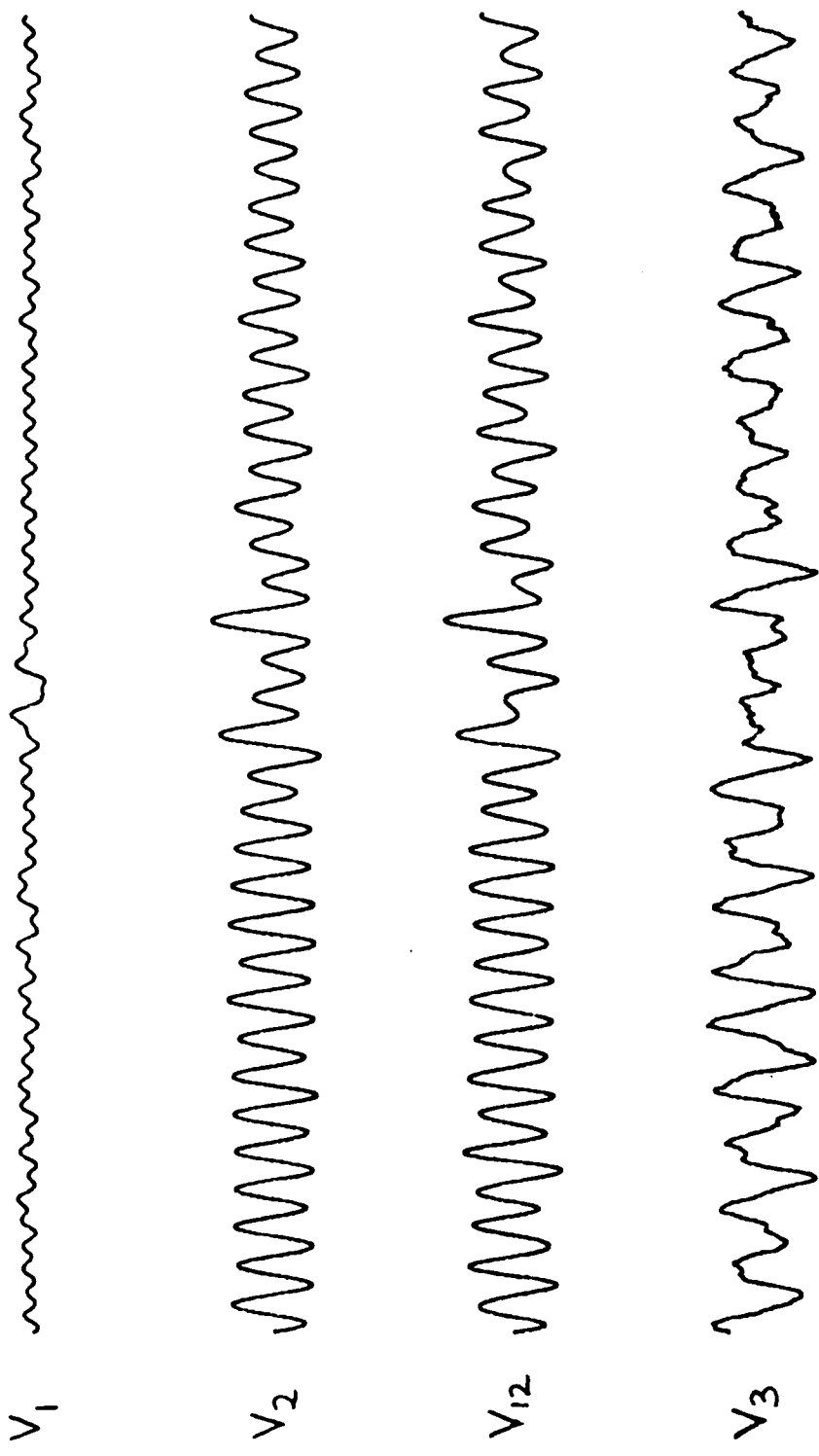
Fig. 21. Signals recorded (see text).

duration $\tau_1 = 60 \, \mu s$. The probe wave had a frequency $f_2 = 1.2 \, MHz$ and duration $\tau_2 = 30 \, \mu s$. The resulting voltage recorded, to be denoted as V_{12} for reasons evident in the discussion below, is actually an average of 512 records obtained under identical conditions. An FFT of this record shows that while there is a significant peak at $f_3 = f_1 - f_2 = 0.8$ MHz, the principal spectral components of V_{12} are at f_1 and f_2.

To enhance the visibility of the signal at f_3 the following background subtraction procedure was introduced. It was desired to subtract from V_{12} those signals associated with the linear scattering of the pump and probe waves which had leaked through the bandpass filter. The following voltage records were obtained by averaging 512 records under conditions which are the same as stated above except as noted: for record V_1 only the pump transducer S_1 was driven while for record V_2 only the probe transducer S_2 was drive. These records are shown in Fig. 21 with the same vertical scale as shown for record V_{12}. Then the record denoted as V_3 was calculated as follows:

$$V_3 = V_{12} - (V_1 + V_2), \tag{27}$$

and the resulting record is displayed in Fig. 21 with an expanded vertical scale.

Figure 22 shows the magnitude of the FFT of V_3. The frequency locations of the principal peaks are identified. The principal spectral component of V_3 is a signal at the difference frequency f_3. This signal is clearly evident by visual inspection of Fig. 21.

The basic assumptions of the background subtraction procedure are that: (i) the signals recorded at frequencies f_1 and f_2 principally come from the linear scattering by the sheet; (ii) there is no significant depletion of these signals due to the interaction of the pump and probe when both are present; and (iii) the propagation related phase delays are truly unchanged during the recording of all three records V_{12}, V_1, and V_2. If these were exactly true, it is to be anticipated that the spectral components in V_3 at the frequencies f_1 and f_2 would be at the same level as the noise. That this is not the case may be a
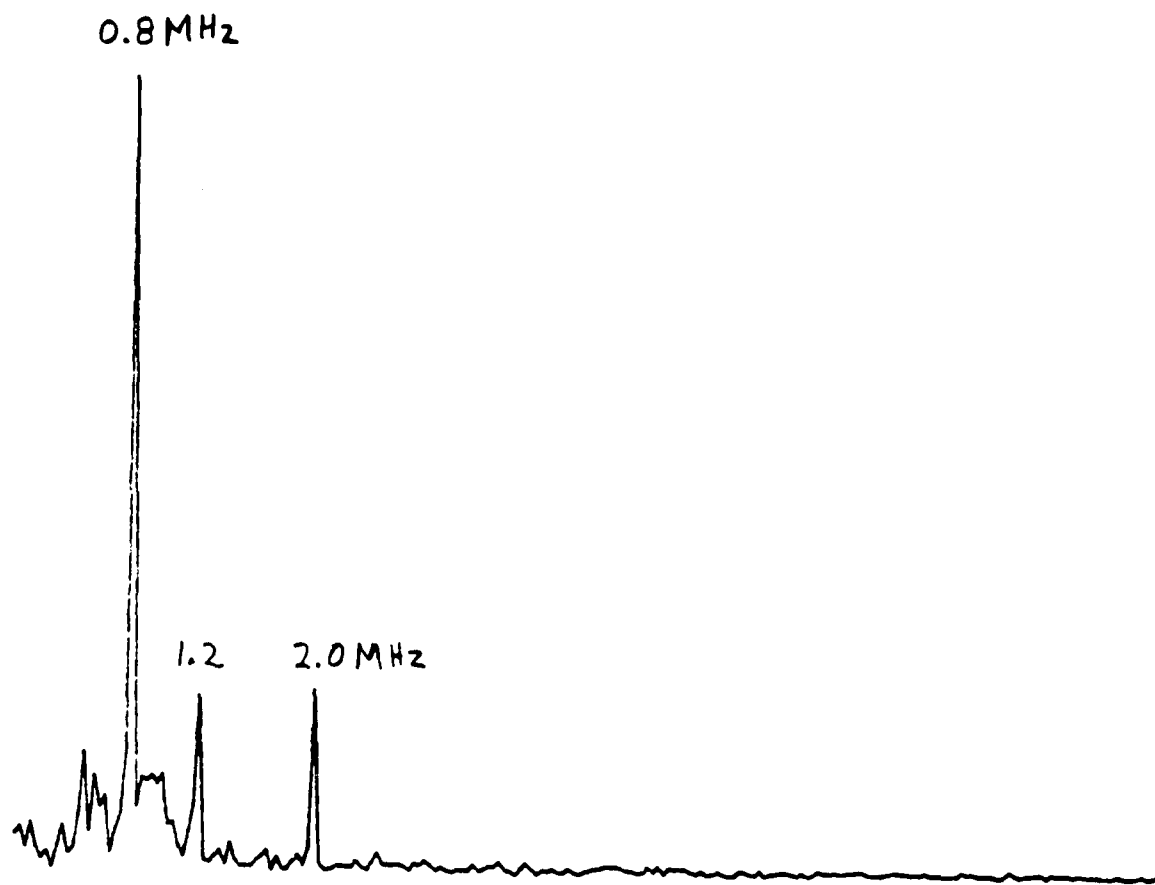
Fig. 22. Spectrum of the background subtracted signal V_3. The principal spectral peak is at the frequency $f_3 = f_1 - f_2$ which is the expected frequency of the reversed wave while the minor peaks are at the pump and probe frequencies f_1 and f_2.

consequence of small displacements of the sheet relative to the transducers. It is anticipated that such displacements will be eliminated with improved mounts though at present such motion may be demonstrated by setting up water waves in the tank. The general success of the background subtraction procedure is evident by considering $<V_j>$, the peak-to-peak amplitude for typical oscillations in each V_j. For $j = 1, 2,$ and 3 these $<V_j>$ are roughly 100 mV, 400 mV, and 60 mV. Inspection of Fig. 22 shows that the contributions to $<V_3>$ from signals at frequencies f_1 and f_2 are down by a factor of 6 to roughly 10 mV. It should be noted that a 60 mV signal at f_3 could not have been caused by a quantization error of the digitizer since the voltage steps of the digitizer is ≈ 1 mV. Calibration to determine the absolute signal magnitude is not presently available.

As of the time of this writing we have not yet been able to explore a range of parameters (such as $f_1, f_2, \tau_1,$ and τ_2 and the position of R_3) so as to optimize the magnitude of signal at f_3. Records with $f_1 = 2.0$ MHz but with $f_2 = 1.4$ MHz gave signals at $f_3 = 0.6$ MHz of the same magnitude. The sheet is asserted to be a few μm in thickness so as to contain bubbles having a spread of resonance frequencies[28] in this range.

In these experiments the probe wave appears to diverge from a "point" at a distance $z_2 \approx 24$ cm from the screen. If the pump wave were a plane wave, Eq. (26) predicts the focal point of the reversed wave would be shifted by a distance $(z_2 - z_3) \approx 8$ cm closer to the screen for the records in Fig. 21. In this case the reversed wave would spread out into a larger fan (than the probe wave) so as to directly intersect R_3. The real pump wave has some curvature which, from the form of Eq. (25), should shift the focus back towards S_2 and reduce the size of the fan. In these experiments the effective source location from the probe wave was offset 10 cm from the axis of the pump beam. It may be advantageous to reduce this offset so that the accuracy of the paraxial approximation, used in the derivation of Eq. (25), is improved.

In the research of Kustov et al.[24,26] the receiver hydrophone was moved to various positions. The dependence of amplitude on position was used to support the claim that the difference frequency wave formed a converging beam. It may be argued however, that a better test for wavefront reversal is to monitor how the *phase* of the difference frequency signal varies with position.[29] Such tests are planned. Additional tests such as these are needed before we can claim to have seen wavefront reversal.

VIII. REFERENCES

1. P. L. Marston, "Propagation and Effects of Acoustical and Optical Waves" (relevant research proposal for the current contract), submitted to O.N.R. Physics Division (Oct. 1, 1985).

2. P. L. Marston, Research proposal submitted to O.N.R. Physics Division (Oct. 1, 1984) for funding period Jan. 1, 1985 - Dec. 31, 1985.

3. P. L. Marston, Annual Summary Report No. 5: Research on Acoustical Scattering, Optics of Bubbles, Diffraction Catastrophes, and Laser Generation of Sound by Bubbles, Accession Number AD-A161333, issued September 1985 (available from the Defense Technical Information Center, Cameron Station, Alexandria, VA).

4. K. L. Williams and P. L. Marston, "Backscattering from an elastic sphere: Sommerfeld-Watson transformation and experimental confirmation," J. Acoust. Soc. Am. 78, 1093-1102 (1985); 79, 2091 (1986).

5. K. L. Williams and P. L. Marston, "Synthesis of backscattering from an elastic sphere using the Sommerfeld-Watson transformation and giving a Fabry-Perot analysis of resonances," J. Acoust. Soc. Am. 79, 1702-1708 (1986).

6. K. L. Williams, Naval Coastal Systems Center (private communication July 1987).

7. K. L. Williams and P. L. Marston, "Axially Focused (Glory) Scattering due to Surface Waves Generated on Spheres: Model and Experimental Confirmation using Tungsten Carbide Spheres," J. Acoust. Soc. Am. 78, 722-728 (1985).

8. D. S. Langley and P. L. Marston, "Glory in the Optical Backscattering from Air Bubbles," Physical Review Letters 47, 913-916 (1981).

9. P. L. Marston, "Cusp diffraction catastrophe from spheroids: generalized rainbows and inverse scattering," Optics Letters 10, 588-590 (1985).

10. M. V. Berry, "Waves and Thom's Theorem," Advances in Physics 25, 1-26 (1976).

11. P. L. Marston, Light Scattering Theory for Bubbles in Water: Inverse Scattering, Coated Bubbles, and Statistics: Final Report Contract N00014-86-K-0242 issued November 1986 (available from Defense Technical Information Center, Alexandria, VA, Accession No. AD-A174997) 55 pages.

12. P. L. Marston, D. S. Langley, and D. L. Kingsbury, "Light Scattering by Bubbles in Liquids: Mie Theory, Physical-Optics Approximations and Experiments," Applied Scientific Research 38, 373-384 (1982).

13. D. S. Langley, Technical Report No. 4: Light Scattering from Bubbles in Liquids, Accession Number AD-A158736 (Defense Technical Information Center, Alexandria, VA, issued December 1984); Ph.D. Dissertation, Washington State University.

14. The sign of the right side of Eq. (23) in Ref. A1 should be reversed.

15. J. A. Kneisly II, "Local curvature of wavefronts in an optical system," J. Opt. Soc. Am. 54, 229-235 (1964).

16. P. L. Marston and E. H. Trinh, "Hyperbolic umbilic diffraction catastrophe and rainbow scattering from spheroidal drops," Nature (London) 312, 529-531 (1984).

17. B. Sturtevant and V. A. Kulkarny, "The focusing of weak shock waves," J. Fluid Mech. 73, 651-671 (1976).

18. W. D. Henshaw, N. F. Smyth, and D. W. Schwendeman, "Numerical shock propagation using geometrical shock dynamics," J. Fluid Mech. 171, 519-545 (1986).

19. M. V. Berry and C. Upstill, "Catastrophe optics: Morphologies of caustics and their diffraction patterns," in *Progress in Optics*, edited by E. Wolf (North Holland, Amsterdam, 1980), Vol. 18, pp. 257-346.

20. F. J. Wright, University of London (Private Communication, 1985).

21. The tank was manufactured by Norwesco Fluid Systems Division, St. Bonifacius, MN.

22. F. J. Hilterman, "Three-dimensional seismic modeling," Geophys 35, 1020 (1970).

23. This technique for imaging sound fields was brought to Marston's attention by L. Hargrove of O.N.R.

24. L. M. Kustov et al., "Phase conjugation of an acoustic wave at a bubble layer," Sov. Phys. Acoust. 31, 517-518 (1985).

25. P. L. Marston, "Focal-point shifts for the reversed wave in acoustical phase conjugation experiments" (abstract), J. Acoust. Soc. Am. Suppl. 82 (to be published in 1987).

26. L. M. Kustov et al., "Nonlinear sound scattering by a bubble layer," Sov. Phys. Acoust. 32, 500-503 (1986).

27. Nuclepore Corporation, 7035 Commerce Circle, Pleasanton, CA 94566-3294.

28. D. L. Miller and E. A. Neppiras, "On the oscillation mode of gas-filled micropores," J. Acoust. Soc. Am. 77, 946-953 (1985).

29. P. L. Marston, Renewal proposal for continuation of this work submitted to O.N.R. in September 1987.

APPENDIX I OF ANNUAL SUMMARY REPORT

SURFACE SHAPES GIVING TRANSVERSE CUSP CATASTROPHES

IN ACOUSTIC OR SEISMIC ECHOES

Philip L. Marston

Department of Physics
Washington State University
Pullman, WA 99164-2814

INTRODUCTION

The reflection of sound from curved surfaces can give rise to cusp
caustics. This paper discusses the theory for locating the cusps and
describes the associated wavefields. The emphasis is on cases where a
cusp caustic opens up roughly transverse to the direction of propagation
of the reflected wave. The present work extends a previous discussion of
such transverse cusps[1] to allow for a wide range of point source and
receiver locations. The concepts of the caustic surface and the
coalescence of adjacent rays and echoes will also be discussed.

During the past decade, considerable advances were made in the
classification of caustics or foci in wavefields. These advances grew out
of the application of the mathematical theory of the singularities of
differential maps (sometimes known as "catastrophe theory") to the
specific mappings which describe rays. The relevant mapping becomes
singular where rays coalesce at caustics and the amplitude of the
wavefield is large near caustics.[2,3] This application of catastrophe
theory is often known as "catastrophe optics". Examples of nontrivial
caustics can easily be demonstrated in the reflection or refraction of
light at smooth surfaces as illustrated by Fig. 6 of the present paper.
The diffraction patterns associated with such caustics are often described
as "diffraction catastrophes" and the effects of diffraction are essential
in determining the local amplitude. Catastrophe optics has recently been
applied to various problems in the far-field scattering of light from
drops of water[4,5] as well as to the fluctuations or twinkling of the
intensity associated with random caustics[2,3].

The methods of catastrophe optics have been applied to various
problems in acoustic[1,6] and seismic[7,8] reflection and propagation.
Information concerning the location and classification of caustics is
useful for reconstructing the local shape of a reflecting surface[7]. The
emphasis of the present paper is not to solve a class of inverse problems
but rather to clarify certain geometric attributes of cusp caustics
associated with reflection. The coalescence and disappearing of rays or
glints as an aperture of an imaging system is scanned across a transverse
cusp curve is also explained. Applications include the reflection of
sound underwater from curved smooth surfaces, sensing of smooth surfaces
with airborne ultrasound, and seismic remote sensing.

LONGITUDINAL AND TRANSVERSE CUSP CAUSTICS

To explain the nature of transverse cusps it is appropriate to review
the better known case of a longitudinal cusp caustic, or "arête",

which opens up roughly along the direction of propagation[3,9]. Figure 1 shows how a curved cylindrical wavefront propagates to produce such a cusp. When point P is chosen (as shown) to lie within the cusp there are three rays (labeled A, B, and C) from points on the initial wavefront to P. As P is shifted down to lie on the adjacent cusp curve, rays A and B merge; if P is shifted to lie outside the cusp there is only one ray to P (ray C for P below the cusp.) If instead of the wavefront shown, we had considered the case of a wavefront corresponding to a sector of a perfect circular cylinder, there would be a perfect line focus at the center of the wavefront. It is therefore common to refer to the cusp focus or caustic, produced by the more typical cylindrical wavefront, as being a consequence of cylindrical aberration.[10] The wavefield near the cusped focus of a cylindrically aberrated wavefront is expressible for monochromatic waves in terms of a one-dimensional diffraction integral; the integral may be expressed in terms of a special function known as the Pearcey function,[10] defined below in Eq. (11).

In contrast to the longitudinal cusp, the transverse cusp caustic opens up roughly transverse to the propagation direction of the wavefront. The relevant geometry is illustrated in Fig. 2. It is supposed that a wave propagates from the exit plane so as to produce a transverse cusp and that the local normals of the initial wavefront are nearly parallel to the z axis. The (u,v) observation plane is taken to be perpendicular to the z axis. In that plane the caustic lies on a cubic cusp curve of the form

$$D(u - u_c)^3 = v^2 , \tag{1}$$

where the parameters D and u_c may depend on the distance z from exit plane to the uv plane and u_c is the u coordinate of the cusp point (which is taken to lie on the u axis).

Evidence for the existence of optical transverse cusps from light scattering experiments[4,5] is reviewed in Ref. 1. Diffraction patterns were observed at large optical distances from water drops in planes perpendicular to the propagation direction of the outgoing light wave. These patterns were observed for oblate drops near the scattering angle of the primary rainbow. For a range of drop shapes, a portion of the diffraction pattern was clearly that of a cusp diffraction catastrophe (which is known to be describable by the Pearcey function.[2]) The conditions of the experiment indicate that a transverse cusp caustic can be established which retains its form even for observation planes infinitely distant from the drop.

GENERIC SHAPE FOR A WAVEFRONT WHICH PROPAGATES TO PRODUCE TRANSVERSE CUSPS

This section reviews pertinent results of a two-dimensional propagation problem[1] giving transverse cusps in the near and far fields of the outgoing wave. The connection with other results of catastrophe theory will be noted. For the purposes of relating the shape of the outgoing wavefront to the location of the caustics, it is convenient to consider a monochromatic wave. In the exit plane (see Fig. 2), the pressure is given by the real part of $p(x,y)\exp(-i\omega t)$ where $p(x,y) = f(x,y) \exp[ikg(x,y)]$, k = $\omega/c>0$, and c is the phase velocity which is assumed to be uniform throughout the region z > 0. Caustic locations which result from this analysis apply also to the problem of a pulsed wave having the same shape of wavefront, as specified by the slowly varying function g(x,y). The analysis can also be used to anticipate caustics in certain situations where the medium is inhomogeneous. Let R denote the distance between representative points having coordinates (x,y) and (u,v) in the exit and observation planes respectively. The Fresnel approximation of the phase shift due to propagation between these points is
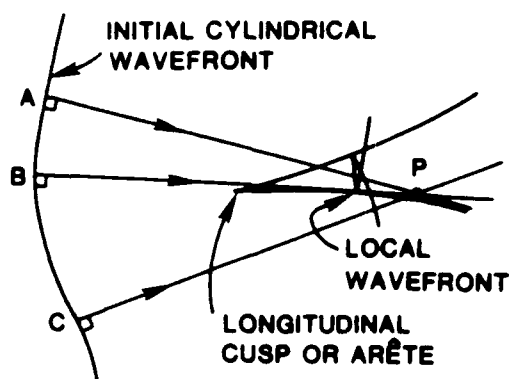
Fig. 1   Propagation of a cylindrical wavefront to form a longitudinal
         cusp caustic.
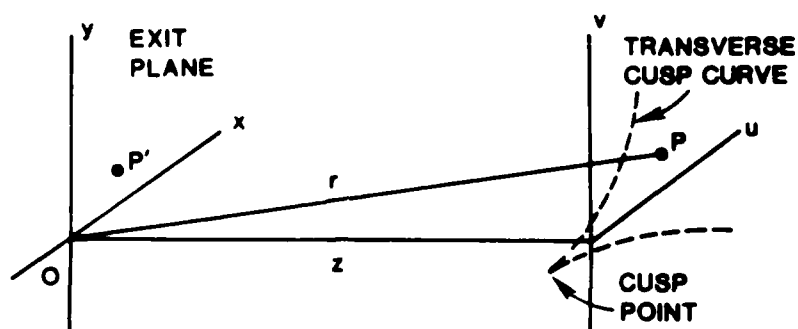
Fig. 2   A wave propagates from the exit plane toward the observation
         plane (u,v). For the problem considered the wavefront near the
         exit plane gives a cusp caustic in the uv plane.
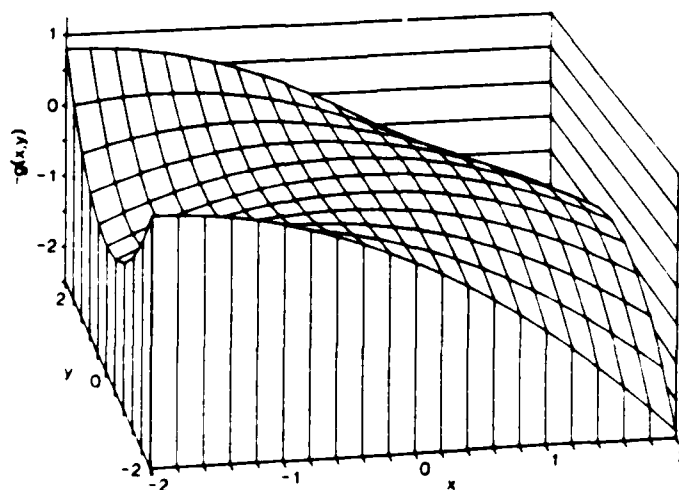
Fig. 3   Plot of -g(x,y) from Eq. (8) with $a_3 = 0$ illustrates an example
         of a wavefront which gives a transverse cusp. The scales are
         in meters by taking $a_1 = 0.2$ m^{-1} and $a_2 = 0.2$m^{-2} or in cm by
         taking $a_1 = 0.2$ cm^{-1} and $a_2 = 0.2$ cm^{-2}.

$$kR \approx kz \left[1 + \frac{1}{2} (U^2 + V^2) \right] - k(xU + yV) + \frac{k(x^2 + y^2)}{2z}, \tag{2}$$

where $U = u/z$ and $V = v/z$ are dimensionless. The Rayleigh-Sommerfeld formulation of scalar diffraction theory reduces to the following approximation for the complex pressure in the (u,v) plane[1]

$$p(u,v) = \frac{k}{2\pi i r} f(x=0, y=0) e^{ikr} F(u,v), \tag{3}$$

$$F = \int\!\!\int_{-\infty}^{\infty} e^{ik\phi(u,v,x,y)} dx dy, \qquad \phi = g(x,y) - (xU + yV) + \frac{(x^2 + y^2)}{2z} \tag{4,5}$$

where the amplitude $f(x,y)$ of the wave in the exit plane can be assumed to be sufficiently slowly varying that it may be well approximated by f evaluated at the origin O of the exit plane. In (3), r denotes the distance from O to (u,v,z) so that the first term in (2) has been approximated as kr. The phase $k\phi$ of the integrand in (4) is stationary where

$$\partial\phi/\partial x = 0 \quad \text{and} \quad \partial\phi/\partial y = 0. \tag{6a,b}$$

If F is approximated using the method of stationary phase, the resulting approximation is equivalent to geometrical optics and gives $F \propto |H|^{-1/2}$ where H is the Hessian[2]

$$H = \frac{\partial^2 \phi}{\partial x^2} \frac{\partial^2 \phi}{\partial y^2} - \left(\frac{\partial^2 \phi}{\partial x \partial y} \right)^2, \tag{7}$$

evaluated for a given (u,v) at the (x,y) which makes (6a) and (6b) true. The method fails at, and near, (u,v) for which $H = 0$. The locus of points giving $H = 0$ define a caustic in the (u,v) plane.

The following choice for $g(x,y)$ yields a transverse cusp specified by (1) with the caustic parameters u_c and D noted below[1]

$$g(x,y) = a_1 x^2 + a_2 y^2 x + a_3 y^2, \tag{8}$$

$$u_c(z) = -2z b_1 b_3 / a_2, \qquad D(z) = 4a_2 / 27 b_1^2 z, \tag{9,10}$$

where $b_1 = a_1 + (2z)^{-1} \neq 0$ and $b_3 = a_3 + (2z)^{-1}$. The conditions on the constants a_j are that $a_2 \neq 0$ and that $-(2a_1)^{-1} \neq z$ for the selected observation plane. Since the parameter a_3 affects only the location u_c of the cusp point, the choice $a_3 = 0$ is allowed. Figure 2 illustrates the cusp's orientation for a case with $a_2 > 0$ and $u_c < 0$. Figure 3 shows a plot of $(-g)$ for representative parameters. In the paraxial approximation the wavefront near the exit plane is advanced along the z direction by a distance $=(-g)$ relative to the exit plane[1]. Hence Fig. 3 illustrates the local shape of an outgoing wavefront which propagates to produce a transverse cusp.

For g specified by (8), the diffraction integral $F(u,v)$ may be expressed using the generalized Pearcey function [1]

$$P_{\pm}(X,Y) = \int_{-\infty}^{\infty} \exp[\pm i(s^4 + s^2 X + sY)] ds, \tag{11}$$

where X and Y are the flowing real-valued linear functions of U and V

$$X = (k/|b_1|)^{1/2}(U_c - U) \operatorname{sgn}(a_2), \quad Y = k^{3/4}|b_1|^{1/4} |2/a_2|^{1/2} V \operatorname{sgn}(b_1) \tag{12}$$

$U_c = u_c/z$, and $\operatorname{sgn}(a_2) = 1$ if $a_2 > 0$ while $\operatorname{sgn}(a_2) = -1$ if $a_2 < 0$. The analysis gives

$$F = (\pi/k|b_1|)^{1/2} e(\mp i\pi/4) \exp(-ikU^2/4b_1) \ J(U,V), \tag{13}$$

$$J = (|b_1|/k)^{1/4}|2/a_2|^{1/2}P_{\pm}(X,Y) \tag{14}$$

where the upper (lower) sign is used if $b_1 < 0$ ($b_1 > 0$); $|P_-(X,Y)| = |P_+(X,Y)|$ so that $|F|$ and the modulus of the diffracted wavefield which decorates the cusp may be obtained from plots[10] of $|P.|$ irrespective of the sign of b_1. At the cusp point $X = 0$, $Y = 0$ so that $|p| \propto k^{1/4}$ and the amplitude diverges in the geometric optics limit, $k \to \infty$.

Discussion of Eq. (8) and relevant results of catastrophe theory is appropriate. For the elementary diffraction catastrophes, the form of the rapidly oscillating integrand of the canonical diffraction integrals is known as a consequence of Thom's theorem.[2,6,7] Unfortunately the shape of the wavefront which propagates to produce a given class of diffraction catastrophe is only specified up to smooth coordinate transformation and the construction of the transformation may not be a trivial task. For the case of a cusp diffraction catastrophe, it is well known that the Pearcey function is the appropriate integral so that for problems in which the diffraction integral is trivially one-dimensional, the shape of the required wavefront follows immediately by inspection of the form of the integrand of (11). For the transverse cusp diffraction catastrophe, reduction of the relevant diffraction integral to a one-dimensional integral is not as trivial so that the salient result of Ref. 1 is that $g(x,y)$ given by (8) is an appropriate two-dimensional (and non-cylindrical) shape. The actual wavefront shape which propagates to produce a transverse cusp is only specified by (8) up to a locally smooth transformation. For example, addition of linear terms $a_4 x + a_5 y$ to the right-hand side of (8) also yields a cubic cusp for the caustic with the cusp point shifted; the analysis given here is applicable with $U = (u/z) - a_4$ and $V = (v/z) - a_5$. It may be argued[1] that the form of (8) is consistent with various results of singularity theory and group theory.

TRANSVERSE CUSPS PRODUCED BY REFLECTION FROM SMOOTH CURVED SURFACES

Before considering the case of reflection of a wave radiated by a point source, it is appropriate to review results from Ref. 1 for the case of monochromatic plane waves incident on a surface whose height, relative to the xy plane, is

$$h(x,y) = c_1 x^2 + c_2 y^2 x + c_3 y^2 + c_4 x + c_5 y, \tag{15}$$

with $c_2 \neq 0$. Throughout this section the amplitude reflection coefficient ξ of the surface is assumed to be such a slowly varying function of the local angle of incidence that it may be well approximated as a constant. Consider first the case where a plane wave of amplitude p_0 is directed vertically downward onto the surface. In the paraxial and Kirchhoff approximations, the reflected wave is equivalent to an upward directed wave in the exit plane having an amplitude $p_0 \xi \exp[ikg(x,y)]$ where $g = -2h(x,y)$. Hence the analysis given in the previous section applies with $a_j = -2c_j$, $j = 1 - 5$, and the reflection will produce transverse cusps. In the case where the plane wave is directed downward at a small angle relative to the vertical, the approximations $a_4 = -2c_4$, and $a_5 = -2c_5$ need to be altered. Transverse cusps can also be produced by reflection from surfaces generated by smooth coordinate transformations of the form given in Eq. (15). This also applies to the case of a point source considered below.

The cusps and wavefields associated with reflection of a wave from a point source will now be analyzed. The geometry is illustrated in Fig. 4. The source is located a distance z_s above the xy plane with an offset from the z axis specified by u_s and v_s. The observation plane is allowed

to differ from that of the source. Discussion will be limited to surface profiles specified by Eq. (15) with $c_4 = c_5 = 0$ since, it may be shown that small linear terms here principally result in linear terms in $g(x,y)$ and a simple shift of the cusp point as noted above. As in the previous discussion, use will be made of a paraxial assumption that the incident and reflected rays are at small angles relative to the z axis. This assumption motivates the Fresnel approximation, as in Eq. (2), of propagation related phase shifts. In this approximation the distance R_s from the source to a given point in the xy plane becomes

$$R_s = (z_s^2 + s^2)^{1/2} = z_s(1 + s^2/2z_s^2), \qquad (16)$$

where $s^2 = (x - u_s)^2 + (y - v_s)^2$. Let $r_s = (z_s^2 + u_s^2 + v_s^2)^{1/2}$ denote the distance of the source from the origin O of the xy plane. The amplitude of the upward directed wave in the exit plane, equivalent to the reflected wave may be approximated as

$$p(x,y) = (q_s^{\xi}/r_s) \exp[ikz_s + ik(s^2/2z_s) - i2kh] \qquad (17)$$

where q specifies the strength of the monopole source. Now the geometry for propagation to the uv plane is as shown in Fig. 2 and it follows that Eq. (3) is replaced by

$$p(u,v) = (kq_s^{\xi}/2\pi i r_s r) \exp[ik(r_s + r)] F(u,v), \qquad (18)$$

where in Eq. (4), Eq. (5) is replaced by

$$\phi = -2h(x,y) - (xU_e + yV_e) + [(x^2 + y^2)/2z_e], \qquad (19)$$

The following effective parameters have been used: $U_e = (u/z) + (u_s/z_s)$, $V_e = (v/z) + (v_s/z_s)$, and $z_e = (z^{-1} + z_s^{-1})^{-1}$. Hence the phase $k\phi$ of the integrand of F has the form previously considered with a_j in Eq. (8) given by $-2c_j$. Inspection of the Eqs. (1), (9), and (10) shows that the caustic location is given by the condition

$$(4a_2/27b_1'^2)(U_e - U_{ec})^3 = V_e^2, \qquad (20)$$

where here the dimensionless effective cusp point location is $U_{ec} = -2b_1'b_3'/a_2$ and $b_j' = -2c_j + (2z_e)^{-1}$. Equation (20) shows that a cusp curve is traced out by varying either (u,v) or (u_s,v_s) while holding the other point fixed. The wavefield is given by Eq. (18) where F is given by Eqs. (11)-(14) with U, U_c, V, and b_j replaced by U_e, U_{ec}, V_e, and b_j', respectively.

To understand the nature of the approximations used in deriving these results, it is helpful to consider the pathological case of reflections form a concave parabolic surface of revolution which corresponds to $c_2 = c_4 = c_5 = 0$ and $c_1 = c_3 > 0$. Inspection of (19) shows that all terms proportional to x^2 and y^2 vanish when the distances of the source and observation planes from the xy plane are such that $z^{-1} + z_s^{-1} = 4c_1$. The caustic degenerates to an image point which is located as per the usual rules of Gaussian or paraxial optics. In this level of approximation the image is point-like since both spherical aberration and the effects of finite aperture size were neglected. The Fresnel approximations, (2) and (16), were important to the derivation. These approximations were also used in the description of the cusps (and associated wavefields), even though the neglected phase terms are not necessarily small for all points on the reflecting surface. This is because it is only necessary for omitted phase terms to be negligible in the xy regions where the stationary phase condition (6) holds.[1] This also justifies other paraxial assumptions used in deriving (17) when the local surface slopes are small near the stationary phase points. Methods of calculating reflected waves more amenable to relaxation of the paraxial assumption and the analysis of transient signals are reviewed in Ref. 7.
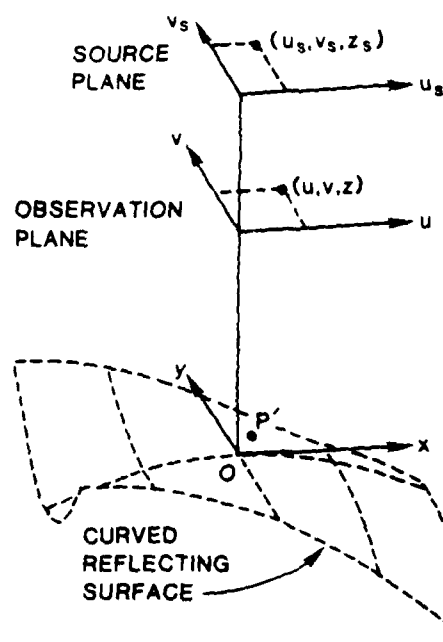
Fig. 4 For the problem considered, the wave from a point source
reflects to give a transverse cusp in the observation plane.
The reflecting surface illustrated has a height relative to the
xy plane of $h(x,y) = c_1 x^2 + c_2 y^2 x$ with $c_1 < 0$ and $c_2 < 0$.
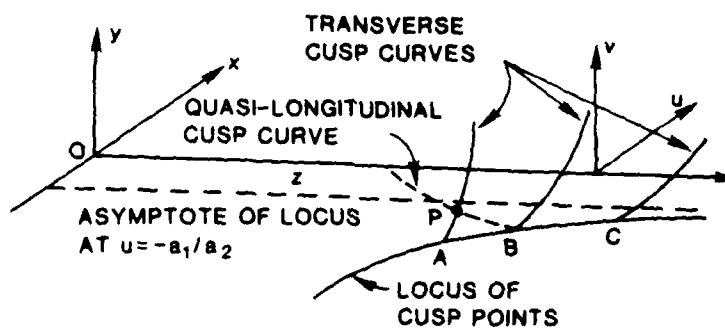
Fig. 5 The caustic surface sketched out from Eq. (1) by varying the distance
z to the observation plane in Eqs. (9) and (10). Point P on that
surface is at the intersection of cusp curves in orthogonal planes.

Fig. 6 Optical simulation of a transverse cusp for the reflection
geometry illustrated in Fig. 4. The screen on the left is the
observation plane and shows the cusp. The curved reflecting
surface is visible in the background.

As the observation plane is moved, the caustic parameters change so that the cusp curve traces out a caustic surface. In the previous section, it was implicit that the reflected wave for the class of surface considered has a shape describable by Eq. (8), with the addition of linear terms. Consequently, the caustic surface of the reflection problem may be displayed by considering the caustic surfaces generated by a suitable class of wavefront shapes. The main features of the caustic surface associated cusps may be seen by omitting linear terms and taking $a_3 = 0$ in Eq. (8). We shall not concern ourselves here with wavefront shapes which cause either a birth or a joining of cusps known respectively as lips and beak-to-beak events.[2,7]

Figure 5 illustrates the main features of the caustic surface for $g = a_1 x^2 + a_2 y^2 x$ with $a_1 > 0$ and $a_2 > 0$. The function $u_c(z)$ gives the locus of cusp points. Inspection of Eq. (9) with the present case of $b_3 = 1/2z$ shows that $u_c \rightarrow u_\infty = -a_1/a_2$ as $z \rightarrow \infty$. Figure 5 shows three transverse cusps in uv planes having three different values of z and having cusp points at A, B, and C. The larger the cusp parameter D in Eq. (1), the faster the transverse cusp curve opens up. Inspection of Eq. (10) shows that for $z \gtrsim (a_1)^{-1}$, D decreases for increasing z. However, when the cusp curve is plotted in the dimensionless coordinates U and V, the corresponding cusp parameter is a constant as $z \rightarrow \infty$; see Eq. (20).

Consider now the intersection of the cusp surface with a plane of constant $u < u_\infty$. That plane intersects the locus of cusp points, say at point B as shown in Fig. 5. The intersection of the plane with the caustic surface traces out a quasi-longitudinal cusp curve, as may be seen from the following analysis. Inspection of Eqs. (1), (9), and (10) shows that the caustic curve in the plane of constant u is

$$-D_L(z - z_c)^3 = v^2, \qquad D_L = D/(2a_2 z z_c)^3, \qquad (21,22)$$

where $z_c = [2a_2(u_\infty - u)]^{-1}$ is the value of z where the locus of cusp points intersects this plane. For z close to z_c, the z dependence of D_L is much slower than that of $(z - z_c)^3$ so that (21) is in essence a cubic cusp curve in the plane of constant u. The factor D_L is positive so the minus sign in (21) indicates that this quasi-cusp opens up in the negative z direction as shown in Fig. 5. Inspection of (22) shows that for $z = z_c > (2a_2)^{-1/2}$, $D_L < D$ so that the longitudinal caustic opens up slower than the transverse cusp having the same cusp point.

The salient differences of the quasi-longitudinal cusp with the longitudinal cusp illustrated in Fig. 1 can be seen by reviewing Fig. 1. By definition, a cylindrical wave is one for which the incident wave retains its shape as the plane of the figure is moved up or down parallel to itself. Furthermore the normal to the cylindrical surface is taken to lie parallel to the plane of Fig. 1. The u axis is taken as normal to this plane; it is therefore normal to the propagation direction. Neither the cusp point location nor the rate at which the cusp opens depend on u. For the quasi-longitudinal cusp, however, both z_c and D_L at $z = z_c$ depend strongly on the choice of the plane of constant u since $z_c \propto (u_\infty - u)^{-1}$ and for u close to u_∞, $D_L \propto (u_\infty - u)^7$.

OPTICAL SIMULATION OF ACOUSTICAL TRANSVERSE CUSPS

Some of the predictions of the previous sections were observed in the qualitative optical reflection experiment shown in Fig. 6. A diverging beam was produced by placing a short-focal-length lens in front of the He Ne laser visible on the right side of Fig. 6. Rays which diverge from this lens simulate those from the point source considered in Fig. 4. A polished mirror-like metal sheet ("Apollo metal") was bent into roughly

the shape shown in Figs. 3 and 4 such that $c_1 < 0$ and $c_2 < 0$. This reflector was placed ~ 1 meter from the focus of the lens such that (u_s, v_s, z_s) ~ (0.1m, 0, 1m). To make the transverse cusp visible, a ground glass screen was placed in the observation plane. Figure 6 was obtained by placing a camera ~ 2m behind the screen and setting the screen ~ 1m from the reflector (z ~ 1m). The orientation of the observed cusp agrees with the predictions of Eq. (20). (For this case $a_2 > 0$ and x and u increase toward the right side of Fig. 6.) Though there appears to be some diffraction related structure near the cusp point, the detailed features of a Pearcey pattern (see e.g. Ref. 1-3) were not resolved, evidently because of relative smallness of the wavelength, 633 nm.

Features evident in Fig. 5 were also observed. For example, quasi-longitudinal cusps and the cusp-point locus were made visible by placing a thin sheet of paper longitudinally in the field of the reflected light. It was found that the asymptote of the cusp-point locus was tilted with respect to the z axis because the source point was displaced from the z axis. Inspection of Eq. (20) shows this behavior is consistent with theory.

LOCATING CAUSTICS BY THE MERGING OF RAYS AND OF PULSED ACOUSTIC ECHOES

Recall from Fig. 1 that the rays from the initial wavefront to a given point P merge if P touches the cusp curve. This section describes rays directed to an observation point P for the case of a transverse cusp (see Fig. 2) and how these rays merge when P touches the cusp. The results are then used to predict the merging of travel times of reflected acoustic pulses. The salient difference between the three rays in Fig. 1 and those to an observer within a transverse cusp is that, in the latter case, the rays don't lie in a plane. This is evident from inspection of Fig. 6 where three glints are visible on the reflecting surface. These glints correspond to rays from the laser source which reflect off of the curved surface into the (narrow) lens aperture of the camera. The camera was purposely placed in the three-ray region such that none of the rays would be blocked by the ground glass screen used to view the cusp.

The procedure for calculating the sites of rays from the exit plane to an observer at P was previously described[1] for g given by Eq. (8). The equations are easily adapted to the geometry of Fig. 4, so only the method will be outlined here. In any problem of this type, the ray sites correspond to the simultaneous roots (x_i, y_i) of Eqs. (6a) and (6b) for an observer at (u, v, z). For the geometry of Fig. 4 the relevant $\phi(U_e, V_e, x, y)$ is given by Eq. (19). For P within the cusp, there are three roots (i = 1, 2, and 3) which corresponds to intersections of a parabola specified by (6a) with a hyperbola specified by (6b). Let P' in Fig. 4 denote a point on the reflector above some point (x, y) in the exit plane; to a distant observer the region around P' appears bright as $(x, y) \rightarrow (x_i, y_i)$. The camera used for Fig. 6 had an aperture situated with u/z = 0. In this case the roots are such that x_1 = x_3, y_1 = $-y_3$, and y_2 = 0; the roots with i = 1 and 3 corresponds to the glints in the upper and lower left, respectively, and i = 2 corresponds to the central glint.

When the camera aperture is placed outside of the cusp, there is only single root and only one glint is visible. The way in which two of the roots disappear is analyzed in Ref. 1 and is consistent with the observed behavior of the glints summarized below. If the camera is moved vertically from its position for Fig. 6, the glints corresponding to i = 1 and 2 move together and merge when the aperture reaches the cusp curve. The merged glints (and corresponding root) disappears as the aperture crosses the cusp curve. Let $\hat{m}$ denote a unit vector in the xy plane parallel to the relative displacement of the merging roots as $(u, v) \rightarrow (u_{cc}, v_{cc})$ where (u_{cc}, v_{cc}) denotes a point on the cusp curve. Let $\hat{n}$ be tangent to the transverse cusp curve at (u_{cc}, v_{cc}). It may be shown that $\hat{m}$ is perpendicular to $\hat{n}$. The observations were in qualitative

agreement with this prediction which suggests a novel method for inferring the orientation of the caustic.

The analysis of ray sites may be used to predict the sequences of pulses received at (u, v, z) for the reflection geometry illustrated in Fig. 4. (The direct pulse from the source is not included in this discussion.) For (u, v, z) in the three ray region, a pulse will be received for each ray, $i = 1$, 2, and 3. Identification of the propagation related phase delays in Eqs. (18) and (19) shows that, from the source to the receiver, the travel time Δt_i for each pulse is such that

$$\Delta t_i\, c = r_s + r + \phi(U_e,\ V_e,\ x = x_i,\ y = y_i). \tag{23}$$

As the points (x_i, y_i) merge when (u, v, z) touches the cusp surface, so will the Δt_i of the corresponding echoes. Only a single echo remains as (u, v, z) is shifted into the one-ray region. The merging of echoes may be used to locate the cusp surface by moving either (u, v, z) or (u_s, v_s, z_s). These features are consistent with previous discussions of seismic echoes from a syncline.[7,11] The detailed impulse response may be inferred from Ref. 6.

ACKNOWLEDGEMENTS

REFERENCES

1. P. L. Marston, Transverse cusp diffraction catastrophes: Some pertinent wavefronts and a Pearcey approximation to the wavefield, J. Acoust. Soc. Am. 81:226 (1987). The sign of the right side of Eq. (23) there should be reversed.
2. M. V. Berry and C. Upstill, Catastrophe optics: Morphologies of caustics and their diffraction patterns, in: "Progress in Optics Vol. 18," E. Wolf ed., North Holland, Amsterdam, (1980).
3. M. V. Berry, Twinkling exponents in the catastrophe theory of random short waves, in: "Wave Propagation and Scattering," B. J. Uscinski, ed., University Press, Oxford, (1986).
4. P. L. Marston and E. H. Trinh, Hyperbolic umbilic diffraction catastrophe and rainbow scattering from spheroidal drops, Nature (London) 312:529 (1984).
5. P. L. Marston, Cusp diffraction catastrophe from spheroids:generalized rainbows and inverse scattering, Opt. Lett. 10:588 (1985).
6. M. G. Brown, The transient wavefields in the vicinity of the cuspoid caustics, J.Acoust.Soc.Am. 79:1367 (1986).
7. G. Dangelmayr and W. Güttinger, Topological approach to remote sensing, Geophys.J.R.Astr.Soc. 71:79 (1982).
8. J. F. Nye, Caustics in seismology, Geophys.J.R.Astr.Soc. 83:477 (1985).
9. A. D. Pierce, "Acoustics, An Introduction to its Physical Principles and Applications," McGraw-Hill, New York (1981).
10. S. Solimeno, B. Crosignani, and P. DiPorto, "Guiding, Diffraction, and Confinement of Optical Radiation," Academic, Orlando (1986).
11. F. J. Hilterman, Three-dimensional seismic modeling, Geophys. 35:1020 (1970).

APRIL 1984

REPORTS DISTRIBUTION LIST FOR ONR PHYSICS DIVISION OFFICE
UNCLASSIFIED CONTRACTS

Director   1 copy
Defense Advanced Research Projects Agency
Attn: Technical Library
1400 Wilson Blvd.
Arlington, Virginia 22209

Office of Naval Research   112   2 copies
Physics Division Office (Code 412)
800 North Quincy Street
Arlington, Virginia 22217

Office of Naval Research   1 copy
Director, Technology (Code 200)
800 North Quincy Street
Arlington, Virginia 22217

Naval Research Laboratory   1 copy
Department of the Navy
Attn: Technical Library
Washington, DC 20375

Office of the Director of Defense   1 copy
Research and Engineering
Information Office Library Branch
The Pentagon
Washington, DC 20301

U.S. Army Research Office   2 copies
Box 1211
Research Triangle Park
North Carolina 27709

Defense Technical Information Center   12 copies
Cameron Station
Alexandria, Virginia 22314

Director, National Bureau of Standards   1 copy
Attn: Technical Library
Washington, DC 20234

Director   1 copy
U.S. Army Engineering Research
and Development Laboratories
Attn: Technical Documents Center
Fort Belvoir, Virginia 22060

ODDR&E Advisory Group on Electron Devices   1 copy
201 Varick Street
New York, New York 10014

Air Force Office of Scientific Research   1 copy
Department of the Air Force
Bolling AFB, DC 22209

Air Force Weapons Laboratory   1 copy
Technical Library
Kirtland Air Force Base
Albuquerque, New Mexico 87117

Air Force Avionics Laboratory   1 copy
Air Force Systems Command
Technical Library
Wright-Patterson Air Force Base
Dayton, Ohio 45433

Lawrence Livermore Laboratory   1 copy
Attn: Dr. W. F. Krupke
University of California
P.O. Box 808
Livermore, California 94550

Harry Diamond Laboratories   1 copy
Technical Library
2800 Powder Mill Road
Adelphi, Maryland 20783

Naval Air Development Center   1 copy
Attn: Technical Library
Johnsville
Warminster, Pennsylvania 18974

Naval Weapons Center   2 copies
Technical Library (Code 753)
China Lake, California 93555

Naval Underwater Systems Center   1 copy
Technical Center
New London, Connecticut 06320

Commandant of the Marine Corps   1 copy
Scientific Advisor (Code RD-1)
Washington, DC 20380

Naval Ordnance Station   1 copy
Technical Library
Indian Head, Maryland 20640

Naval Postgraduate School   1 copy
Technical Library (Code 0212)
Monterey, California 93940

Naval Missile Center   1 copy
Technical Library (Code 5632.2)
Point Mugu, California 93010

Naval Ordnance Station   1 copy
Technical Library
Louisville, Kentucky 40214

Commanding Officer   1 copy
Naval Ocean Research & Development Activity
Technical Library
NSTL Station, Mississippi 39529

Naval Explosive Ordnance Disposal Facility   1 copy
Technical Library
Indian Head, Maryland 20640

Naval Ocean Systems Center   1 copy
Technical Library
San Diego, California 92152

Naval Surface Weapons Center   1 copy
Technical Library
Silver Spring, Maryland 20910

Naval Ship Research and Development Center   1 copy
Central Library (Code L42 and L43)
Bethesda, Maryland 20084

Naval Avionics Facility   1 copy
Technical Library
Indianapolis, Indiana 46218

END

12 - 87

DTIC